A human TRPV1 genetic variant within the channel gating domain regulates pain sensitivity in rodents

Shufang He,[1,2#] Vanessa O. Zambelli, [2,3#] Pritam Sinharoy,[2] Laura Brabenec,[4] Yang Bian,[2] Freeborn Rwere,[2] Rafaela C.R. Hell,[2] Beatriz Stein Neto,[2,3] Barbara Hung[2], Xuan Yu[2], Meng Zhao[5,6,7], Zhaofei Luo,[1] Chao Wu,[1] Lijun Xu,[2], Katrin J. Svensson,[5,6,7] Stacy L. McAllister,[2,8] Creed M. Stary,[2] Nana-Maria Wagner,[4] Ye Zhang,[1] Eric R. Gross[2,6,7*]

[1]Department of Anesthesiology and Perioperative Medicine, the Second Hospital of Anhui Medical University; Key Laboratory of Anesthesiology and Perioperative Medicine of Anhui Higher Education Institutes, Anhui Medical University, Hefei, China.

[2] Department of Anesthesiology, Perioperative and Pain Medicine, School of Medicine, Stanford University, Stanford, CA, USA

[3] Laboratory of Pain and Signaling, Butantan Institute, São Paulo, Brazil.

[4] Department of Anesthesiology, Intensive Care and Pain Medicine, University Hospital Münster, Münster, Germany

[5] Department of Pathology, School of Medicine, Stanford University, Stanford, CA, USA.

[6] Stanford Diabetes Research Center, School of Medicine, Stanford University Stanford, CA, USA

[7] Stanford Cardiovascular Institute, School of Medicine, Stanford University, CA, USA

[8] Department of Obstetrics & Gynecology, School of Medicine, Emory University, Atlanta, Georgia.

[#] These authors contributed equally to this paper.

[*]**Correspondence author**: Eric R. Gross, MD, PhD, Department of Anesthesiology, Perioperative and Pain Medicine, School of Medicine, Stanford University, Stanford, 300 Pasteur Drive, CA, 94305-5640. Tel: 1-650-723-7442; Email: ergross@stanford.edu

Conflict-of-interest statement: ERG has a patent on "Peptide modulators of specific calcineurin protein-protein interactions" (US Application Serial No. 16/082,313) that includes the V1-cal peptide. The other authors have declared that no conflict of interest exists.

Abstract

Pain signals are relayed to the brain *via* a nociceptive system, and in rare situations, this nociceptive system contains genetic variants that can limit pain response. Here we questioned whether a human transient receptor potential vanilloid 1 (TRPV1) missense variant causes a resistance to noxious stimuli and further if we can target this region by a cell-permeable peptide as a pain therapeutic. Initially using a computational approach, we identified a human K710N TRPV1 missense variant in an otherwise highly conserved region of mammalian TRPV1. After generating a $TRPV1^{K710N}$ knock-in mouse using CRISPR/Cas9, we discovered the K710N variant reduced capsaicin-induced calcium influx in dorsal root ganglion neurons. The $TRPV1^{K710N}$ rodents also had less acute behavioral response to chemical noxious stimuli and less hypersensitivity to nerve injury, while leaving the response to noxious heat intact. Furthermore, blocking this K710 region in wild-type rodents by a cell-penetrating peptide limited acute behavioral responses to noxious stimuli and rescued pain hypersensitivity induced by nerve injury back to baseline. These findings identify K710 TRPV1 as a discrete site crucial for the control of nociception and provides insights into how to leverage rare genetic variants in humans to uncover fresh strategies for developing pain therapeutics.

Introduction

Pain afflicts over 1.5 billion individuals worldwide and costs more than $600 billion annually in United States alone (1). Secondary health problems from treating pain, including opioid abuse, dependence, and overdose are fueling an opioid epidemic that is complicated by the present COVID-19 endemic (2). To address the human health problem of pain and the secondary impact caused by opioid dependence, addiction, and overdose, there is an unmet need to further understand how the nociceptive system perceives pain and how genetic variants within the nociceptive system may alter the intensity of this nociceptive signal. This could provide important insights which can assist with developing therapeutics to limit pain.

In humans, documented missense or nonsense variants (as in the case for extremely rare Nav1.7 channel variants) can alter a pain response substantially. This can result in modifying the nociceptive system and nociceptive response to be at the two different ends of the pain spectrum- where a gain of function variant can cause extreme pain disorder and a loss of function variant a complete inability to experience pain (3-5). This example also highlights that introducing a complete loss of function variant into a nociceptor could be detrimental as sensing a noxious insult and withdrawing (such as when a hand is placed on a hot stove) is an important physiological function to limit cellular injury. Largely unexplored are the over one thousand reported human genetic variants within the transient receptor potential vanilloid 1 (TRPV1) channel- a channel that is highly expressed in nociceptive sensory neurons which detects noxious stimuli leading to pain perception and transmission (6). Past investigations have shown that the blockade of TRPV1 channel could alleviate pain behaviors, but most TRPV1 antagonists suffered from side effects such as abnormal temperature regulation and loss of noxious heat response (7). *In vitro* site-mutagenesis studies showed that point mutations can selectively eliminate TRPV1 activation but leave heat sensing intact, implying such modality-selective antagonists could be a more attractive approach for pain therapeutics (8, 9).

Recently, advances including a cryoEM TRPV1 structure (10) and CRISPR/Cas9 technology for gene editing have provided opportunity to further investigate human TRPV1 genetic variants. A CRISPR/Cas9 gene editing system has recently been demonstrated to provide a long-lasting pain relief *via* precisely targeted *in vivo* epigenetic repression of the Nav1.7 channel (11). This implies the CRISPR-based gene therapy could lead to an opioid-free way of treating pain (12). Additionally, one strategy to uncover human TRPV1 variants that may reduce pain responses could involve turning to birds. This is because within nature avian species, unlike mammals, possess a TRPV1 receptor that is naturally resistant to noxious insults yet can still perceive pain and trigger protection from injuries such as a heart attack (13, 14). This is important to consider when investigating TRPV1 genetic variants as recent evidence also suggests TRPV1 in non-neuronal cells serves as an intracellular molecular sensor protecting from glucose-induced cellular stress or tissue ischemia (15, 16). Here, we hypothesize that by using the human TRPV1 missense variants identified through genetic sequencing when coupled with the genetic divergence in avian species relative to mammals, we can pinpoint a region to genetically manipulate the mammalian TRPV1 receptor using CRISPR/Cas9, to reduce, yet not eliminate, TRPV1-mediated responses to pain without exacerbating cellular injury. If successful, we can then develop a cell permeable peptide to target this region to reduce acute and chronic pain responses.

Results

Identification of human missense TRPV1 variants that cause a genetic divergence to avian TRPV1

Within the gnomAD database, 1461 variants were identified from 281,434 *TRPV1* alleles. We excluded the 259 synonymous variants and 542 other type variants that did not result in a missense or loss of function. The remaining 580 missense variants and 80 predicted loss of function variants for human *TRPV1* were then compared with avian *TRPV1*, which genetically diverged much earlier from mammals (Supplemental Figure S1). To understand the basis for this divergence, multiple sequence alignment identified 62 amino acids that differ when comparing avian with mammalian *TRPV1*(Supplemental Figure S2). When comparing this to the human *TRPV1* variants from the gnomAD database, we identified 5 missense variants that caused human *TRPV1* to genetically revert back to avian *TRPV1* (Figure 1A).

For these 5 missense variants, we identified their location using cryo-EM TRPV1 structure (PDB ID: 3J5P) (10). Of most interest was the variant identified within the C-terminus TRP domain (residues 687-711), which is located just after the sixth transmembrane segment and has been proposed to engage in channel gating(10). This region forms an intracellular α-helix parallel to the cell membrane (Figure 1B). Interestingly, just past the evolutionary conserved TRP box (residues 696-701), the avian TRPV1 diverges from mammalian species and has two residues, I708 and N710, different from the mammalian T708 and K710 (Figure 1B). When the structure is analyzed based on the cryo-EM TRPV1, the K710 residue forms hydrogen bonds with S711 and L706 (red dashed lines), while T708 residue forms hydrogen bonds with T704 and I705 (blue dashed lines) (Figure 1C).

To examine this further and to mimic the avian TRP domain sequence, we performed K710N and T708I substitutions using Chimera. The replacement of K710 to N710 causes changes in hydrogen bond interactions with neighboring amino acids. The N710 residue does not interact with

S711, instead it contacts with C-terminal K714 and E397 in the linker region (Figure 1C). In contrast, T708I substitution does not change its interactions with T704 and I705, while forming two more hydrogen bonds with S711 and D707 within the TRP domain (Figure 1C). This evolutionary and *in silico* data suggest that in avian species the residues of N710 and I708, genetically divergent relative to mammalian K710 and T708, cause different structural changes in a region just past the TRPV1 TRP box that regulates TRPV1 gating (17). As such, we next determined whether these changes lead to functional differences in the TRPV1 channel.

TRPV1 site-directed mutagenesis at K710 decreases capsaicin-induced calcium influx

Since the K710N missense variant in humans is quite rare (1.6×10^{-5} frequency), to explore whether K710N will affect the channel function for TRPV1, we performed site-directed mutagenesis. K710N, T708I, and T708I/K710N mutations were constructed from a wild type rat TRPV1 plasmid (Supplemental Table S1) and transfected into H9C2 cells, which lack endogenous TRPV1 cell surface expression. The K710N transfected cells treated with capsaicin (1μM, a selective and specific TRPV1 agonist), reduced the total amount of calcium influx (area under curve, AUC) by 4.4-fold compared to wild type TRPV1 transfected cells (Figure 1D, 1E, 1H, 4.66±1.14 vs. 20.45±2.95 arbitrary units, respectively, $p<0.0001$). In contrast, the T708I mutation caused a 1.8-fold increase in intracellular calcium influx relative to wild type TRPV1 cells (Figure 1D, 1F, 1H 36.90±1.15 vs. 20.45±2.95 arbitrary units, respectively, $p<0.0001$). However, the T708I/K710N double mutation caused 1.7-fold less calcium influx than wild type TRPV1 cells following capsaicin stimulation (Figure 1D, 1G, 1H, 11.93±2.44 vs. 20.45±2.95 arbitrary units, respectively, $p=0.0342$).

The peak intracellular calcium after capsaicin was also decreased in K710N TRPV1 cells relative to wild type TRPV1 cells (Figure 1I, 28±6% vs. 100±11%, % of wild type, respectively, $p<0.0001$). The cells transfected with T708I TRPV1 had a similar peak intracellular calcium rise

to wild type TRPV1 cells while the peak was lower for the T708I/K710N TRPV1 double mutation (Figure 1I, T708I: 117±6%, T708I/K710N: 63±11%, vs. 100±11% in wild type TRPV1, % of wild type). Together, these data suggest that K710N TRPV1 reduces capsaicin-induced calcium influx in transiently transfected H9C2 cells.

Generation of CRISPR/Cas9 edited TRPV1^{K710N} knock-in mice

To investigate whether the K710N TRPV1 point mutation alters behavior to noxious insults including capsaicin *in vivo*, we generated a TRPV1^{K710N} knock-in mouse using CRISPR/Cas9 (Figure 2 A). Three guide RNAs (gRNAs) were designed near the K710 site located in Exon 14 of the mouse TRPV1 locus (Supplemental Table S2). Both gRNA1 and gRNA2 can cut efficiently, and the gRNA1 was used for mouse zygote injection. The donor single-stranded oligodeoxynucleotide (ssODNs) contains a missense mutation for K710N (red base), and two silent mutations (green bases) in gRNA protospacer adjacent motif (PAM) site (purple bases), to block the PAM sequence in order to prevent re-cutting of corrected mutated allele by gRNA-Cas9 (18) (Figure 2A). The gRNA together with the mutation containing ssODNs, and Cas9 protein were co-injected into the pronucleus of C57BL/6J zygotes and implanted into recipient mothers. A total of 16 pups were born and CRISPR/Cas9 mediated editing occurred in all pups as examined by T7 endonuclease I (T7EI) cleavage assay (Supplemental Figure S3A and 3B). Six mice bearing the designed mutation were identified from 16 pups, as determined by DNA sequencing (Supplemental Figure S3C). Of those, we identified a founder mouse without a non-homologous end joining (NHEJ) mutation and with only the desired G>C point mutation to produce a TRPV1 K710N mutation. We backcrossed the TRPV1^{K710N} mouse with C57BL/6J wild type mice and then inbred for heterozygous (double peak) and homozygous (single peak) offspring, which were verified by DNA sequencing (Figure 2B). After intercrossed for three generations, the fourth generation TRPV1^{K710N} homozygous mice were used for testing. Eighth generation offspring of TRPV1^{K710N} mice were sent to Charles River (France) for rederivation and the vascular studies were performed

using the TRPV1^{K710N} homozygous mice in the Wagner laboratory (mouse was a gift from Dr. Eric R. Gross, Stanford University, Stanford, California). The TRPV1^{K710N} mice were also generated at Shanghai Model Organisms Center Inc. (Shanghai, China) and used to reproduce a portion of the DRG studies in the He laboratory. The TRPV1^{K710N} mice were viable, fertile, and exhibited normal motor activity when subjected to rotarod testing relative to wild type mice (Supplemental Figure S4A and 4B). In addition, the TRPV1^{K710N} mice showed intact response to noxious heat (48°C and 55°C), with similar withdrawal latency relative to wild type mice in a tail immersion test (Figure 2C, 48°C: 7.7±0.9 vs. 6.7± 0.9 sec, p=0.4561). The body temperature detected by a rectal thermal probe was also not different between the wild type TRPV1 and TRPV1^{K710N} mice (Figure 2D, 38.0±0.03 vs. 37.9±0.07 °C, p=0.2006). When considering sex as a biological variable, no differences were seen for these temperature studies (Supplemental Figure S5A and 5B).

TRPV1 ^{K710N} knock-in mice are resistant to capsaicin-elicited nocifensive behavior

Next, we challenged the wild type TRPV1 and TRPV1^{K710N} mice with bird food laced with capsaicin. This type of food is typically used by chicken farmers as the capsaicin prevents mammals, such as squirrels, from eating the food while the chickens eat *ad libitum*. Unexpectantly, by placing the bird food on the floor of the cage, this resulted in a rodent behavioral response, including rodents lifting their paws off the bird food in response to the dermal absorption of capsaicin. We quantified this behavioral response between the wild type TRPV1 and TRPV1^{K710N} mice by monitoring paw withdrawal (where at least three paws are on the cage wall or jumping) after exposure to the bird food with capsaicin. When exposed to the bird food containing capsaicin (Sizzel N'Heat), the wild type mice exhibited more nocifensive behavior compared to the TRPV1^{K710N} mice (Figure 2E, Supplemental Movie S1). Paw withdrawal from the food was markedly increased for wild type TRPV1 mice relative to the TRPV1^{K710N} mice (Figure 2F, 50±6 vs.15±6 instances of paw withdrawal/10 min, respectively, p<0.0001). In contrast, when exposed

to the bird food without capsaicin (Porch N'Patio) both mice do not exhibit this behavior (Supplemental Movie S2). The paw withdrawal was similar between wild type TRPV1 and TRPV1^{K710N} mice (Figure 2F). When considering sex as a variable, no differences were identified in behavior between male and female mice (Supplemental Figure S5C).

We then examined the nociceptive behavior triggered by intraplantar capsaicin injection (Figure 2G). Nociceptive behaviors (paw-licking/flinching) after capsaicin injection were reduced in TRPV1^{K701N} mice relative to wild type TRPV1 mice (Figure 2H, 27±4 vs. 57±6 sec, respectively, p=0.0004). The wild type TRPV1 mice exhibited nociceptive behaviors including paw-licking and flinching over 2 min after capsaicin injection (Supplemental Movie S3). In comparison, TRPV1^{K701N} mice showed less nociceptive behaviors, mostly in the first 30 sec after capsaicin injection (Supplemental Movie S4). After vehicle injection, there is no significant difference for paw-licking/flinching time between the two groups (Figure 2H). When considering sex as a biological variable, no differences were noted between male and female rodents (Supplemental Fig 5D). We also evaluated the pain behavior induced by Brp-LPA, an analogue of lysophosphatidic acid (LPA), that induces acute pain by directly interacting with TRPV1 at K710 site (19). Nociceptive behaviors induced by Brp-LPA was markedly decreased in TRPV1^{K710N} mice compared to those of wild type TRPV1 mice (Supplemental Figure S6). As we did not identify any sex differences between male and female mice, we used male mice for the remainder of the study.

Capsaicin injection induces neurogenic inflammation, causing vasodilation and tissue edema (20). Following intraplantar capsaicin injection, paw thickness was also reduced in TRPV1^{K701N} mice relative to wild type TRPV1 mice (Figure 3A). Blood flow measured by laser doppler flowmetry was also markedly increased following capsaicin injection in wild type TRPV1 mice, which was less in TRPV1^{K701N} mice (Figure 3B and 3C). Pressure myography of mesenteric resistance arteries from wild type TRPV1 and TRPV1^{K701N} mice also identify that arteries from

TRPV1^{K710N} mice have a reduced vasodilatory response to capsaicin compared to wild type TRPV1 mice (Figure 3D and 3E).

We then cultured primary DRG neurons from wild type TRPV1 and TRPV1^{K701N} mice. Different responses to capsaicin-induced calcium influx in wild type and TRPV1^{K710N} mice were observed (Figure 4A and 4B). The capsaicin-induced area under the curve was reduced in TRPV1^{K710N} DRG compared to those of wild type TRPV1 DRG (Figure 4C, 9.8±1.9 vs. 18.0±3.3 arbitrary units, respectively, p=0.022). The peak intracellular change in Fura-2 AM was also 41% lower in TRPV1^{K710N} DRG cells relative to wild type TRPV1 DRG cells (Figure 4D, 59±8% vs. 100±15%, % of wild type, respectively, p=0.016). These findings for the TRPV1^{K710N} and wild type TRPV1 mice was also reproduced in a separate laboratory (Supplemental Figure S7A-7D).

We next examined the colocalization of TRPV1 with IB4 and CGRP in DRG neurons from wild type TRPV1 and TRPV1^{K710N} mice (Figure 4E). The total percentage of IB4-positive neurons were not different between the wild type TRPV1 and TRPV1^{K710N} mice (Figure 4F). However, the number of IB4-positive neurons expressing TRPV1 in TRPV1^{K710N} mice was significantly reduced compared to the wild type TRPV1 mice (Figure 4G, 6.2±1.3 vs.16.5±1.9%, respectively, p=0.0004). Although there were no differences in the total number of CGRP neurons (Figure 4H) and the number of CGRP-positive neurons expressing TRPV1 (Figure 4I), the CGRP intensity was decreased in DRG neurons from TRPV1^{K710N} mice relative to wild type TRPV1 mice (Figure 4J).

TRPV1^{K710N} mice have attenuated hypersensitivity from nerve injury

Wild type TRPV1 and TRPV1^{K710N} mice were subjected to the spared nerve injury (SNI) (21), and the mechanical and thermal sensitivity were measured at designated time points (Figure 5A). The nerve injury shortened thermal latency in both mice, but the thermal hypersensitivity in TRPV1^{K710N} mice was partly recovered from the 7th day after surgery. There was no significant difference between the sham and SNI group of TRPV1^{K710N} mice at day 10 and 14 after surgery (Figure 5B). The wild type TRPV1 mice had a significantly lower mechanical withdrawal threshold

at day 3 after SNI injury relative to rodents with a sham procedure (Figure 5C, 0.10±0.03 vs. 0.90±0.13 g, p=0.0016), with mechanical hypersensitivity continued for the two weeks of testing. In contrast, TRPV1^{K710N} mice exhibited less of an impact than the wild type TRPV1 mice when assessing withdrawal threshold over the course of 2 weeks (Figure 5C, 1.14±0.07 vs. 0.20±0.07 g at day 14, respectively, p<0.0001). Further, the percent mechanical hypersensitivity relative to the uninjured paw was significantly reduced in TRPV1^{K710N} mice relative to wild type TRPV1 mice (Figure 5D, 24±7 vs. 89±5 % at day 14, respectively, p<0.0001). These data suggest that K710N mutation reduces nerve injury-induced pain hypersensitivity.

TRPV1^{K710N} knock-in mice are resistant to cellular injury

Besides transmitting a nociceptive signal to the brain, the TRPV1 channel also contributes an important role in regulating cellular injury that is independent of the nervous system (22-24). We further examined if the TRPV1 K710N variant, as it limits calcium-induced cellular influx, exacerbates cellular injury in isolated cardiomyocytes (that are devoid of a nervous system) when subjected to hydrogen peroxide (H_2O_2) or hypoxia/reoxygenation. After exposure to H_2O_2, the percentage of calcein-AM stained viable cells was greater in TRPV1^{K710N} cells relative to wild type TRPV1 cells (Figure 6A and 6B, 84±4 vs. 57±6%, % of control, p=0.0001). In contrast, the propidium iodide (PI) stained dead cells were reduced in TRPV1^{K710N} cells compared to wild type cells (Figure 6A and 6C, 133±8 vs. 176±15 %, % of control, p=0.0107). Additionally, thiazolyl blue tetrazolium bromide (MTT) assay showed that cell viability in TRPV1^{K710N} cells was higher than those of wild type cells (Figure 6D, 85±2 vs. 72±4 %, % of control, respectively, p=0.0010). Following hypoxia/reoxygenation injury, TRPV1^{K710N} cardiomyocytes had more calcein-AM stained viable cells and less PI-stained dead cells, as well as increased cell viability relative to wild type cells (Supplemental Figure S8A-8D).

We further examined the glycolytic function of the cardiomyocytes by using a Seahorse extracellular flux analyzer as a mechanism to why TRPV1^{K710N} cells are tolerant to cellular injury.

The response to glycolytic stress, as evaluated by measuring extracellular acidification rate (ECAR) under glucose, oligomycin and 2-deoxy-glucose (2-DG), was different between the wild type and TRPV1^{K710N} cells (Figure 6E). When analyzing the glycolytic function, the glycolytic capacity was significantly increased in TRPV1^{K710N} cardiomyocytes as compared with the wild type cardiomyocytes (Figure 6F, ECAR: 15.40±1.18 vs. 9.30±1.17 mPH/min, p=0.0063). The glycolytic reserve of TRPV1^{K710N} cardiomyocytes was also higher than those of wild type cells (Figure 6G, ECAR: 4.92± 0.98 vs. 1.34±0.52 mPH/min, p=0.0119). No differences between the two mice were observed for non-glycolytic acidification and glycolysis (Figure 6H and 6I).

As we noted that the TRPV1^{K710N} mice have elevated glycolytic reserve and as the primary fuel source for the brain is glucose, we also questioned whether these mice were resistant to stroke in a focal cerebral ischemia model of 1-hour transient middle cerebral artery occlusion (MCAO) followed by 24 hours reperfusion. Cerebral infarct size in TRPV1^{K710N} mice was significantly reduced relative to wild type mice (Supplemental Figure S8E and 8F, 18± 3 vs. 29±3 %, respectively, p=0.0234). Together, these observations demonstrate the TRPV1^{K710N} mice produce a beneficial effect of enhancing glycolytic function and decreasing injury from oxidative stress and ischemia even though there is a reduced behavioral response to pain.

A peptide targeting the TRPV1 K710 region limits capsaicin-induced nocifensive behavior and chronic pain from nerve injury

Since the TRPV1^{K710N} mouse did not exacerbate organ injury while also reducing, yet not eliminating nocifensive responses to noxious insults, based on the structure of native mammalian TRPV1, we developed a peptide ($_{701}$RAITILDTEKS$_{711}$) which spans the α-helix that contains K710 that is just past the evolutionary conserved TRP box. As this region is an intracellular helix which runs parallel to the membrane, the peptide was conjugated to TAT$_{47-57}$ for intracellular entry and the peptide was named V1-cal (23).

V1-cal or TAT_{47-57} were preinjected into the paw 15 min before capsaicin or vehicle intraplanar injection (Figure 7A). Treatment with either TAT_{47-57} or V1-cal alone did not elicit a behavioral response in wild type TRPV1 rodents (Figure 7B, 2.9±0.5 and 4.3±0.9 sec, respectively). When subjecting wild type TRPV1 mice to acute capsaicin, V1-cal substantially reduced the nociceptive response to capsaicin relative to the TAT_{47-57} vehicle-treated rodents (Figure 7B, 32.8±4.4 vs. 86.0±6.9 sec, respectively, $p<0.001$). Brp-LPA-induced responses in wild type TRPV1 mice were also reduced by pretreatment of V1-cal (Supplemental Figure S9). Moreover, V1-cal reduced capsaicin-induced paw swelling as opposed to TAT_{47-57} (Figure 7C). V1-cal also reduced capsaicin-mediated blood flow changes relative to TAT_{47-57} treatment (Figure 7D, 7E). The vasodilative response to capsaicin was also markedly attenuated by V1-cal but not TAT_{47-57} (Figure 7F, 7G). Since TRPV1 antagonists can trigger an increase in body temperature, we further measured the rectal temperature after V1-cal or TAT_{47-57}. V1-cal or TAT_{47-57} had little effect on body temperature, as compared to AMG9810, a TRPV1 antagonist, which increased temperature after injection (Figure 7H, 7I).

We then cultured primary DRG neurons from wild type TRPV1 mice and perfused DRG neurons with V1-cal (1μM) or TAT_{47-57} (1μM) 10 minutes prior to capsaicin (1 μM, 15 sec) and up until the end of capsaicin treatment. Different responses to capsaicin-induced calcium influx in TAT_{47-57}-treated relative to V1-cal treated DRG were observed (Figure 8A and 8B). The capsaicin-induced area under the curve was reduced in V1-cal treated DRG compared to TAT_{47-57}-treated DRG (Figure 8C, 7.6±1.5 vs. 47.8±10.3 arbitrary units, respectively, $p<0.0001$). The peak intracellular change in Fura-2 AM was also 69% lower in V1-cal treated DRG cells relative to TAT_{47-57} treated DRG cells (Figure 8D, 31±5% vs. 100±16%, % of TAT_{47-57}+capsaicin, respectively, $p=0.0001$).

As capsaicin can alter the expression of neuropeptides in TRPV1-positive sensory neurons (25), we examined the expression of SP and CGRP in DRG tissues 20 min after intraplantar

capsaicin injection in TAT_{47-57}-treated and V1-cal-treated mice. The capsaicin-induced upregulation of SP and CGRP in DRG neurons was decreased in the V1-cal-treated group when compared to TAT_{47-57} -treated group (Figure 8E, 8F, 8G).

As drugs targeting TRPV1 may lead to unwanted temperature changes, we implanted mice with a subcutaneous temperature probe to measure body temperature in awake freely moving mice. After acquiring 2 days of baseline temperature data, we implanted rodents with osmotic pumps with TAT_{47-57} vehicle or V1-cal. Body temperature measured over the subsequent 12 days showed that V1-cal had no apparent impact on rodent body temperature (Supplemental Figure S10).

Therefore, we further questioned whether delivering the V1-cal peptide through an osmotic pump could rescue the behavioral changes in the spared nerve injury model in wild type mice. Two weeks after surgery, the mice subjected to spared nerve injury were randomly chosen to receive *via* an osmotic pump TAT_{47-57} vehicle or V1-cal (Figure 9A). Few changes were noted in thermal latency for the spared nerve injury rodents relative to sham-treated rodents during the injury phase or rescue phase (Figure 9B). The rodents subjected to spared nerve injury significantly had a lower mechanical withdrawal threshold during the injury phase relative to rodents with a sham procedure (Figure 9C, 0.13±0.04 vs. 1.32±0.15 g, respectively, $p=0.0003$). Further, during the rescue phase, the subset of the spared nerve injury rodents given V1-cal had a substantial reversal of mechanical withdrawal threshold as opposed to rodents treated with TAT_{47-57} (Figure 9C, 1.25±0.25 vs. 0.30±0.03 g, respectively, $p=0.0144$). This reversal was comparable to the mechanical threshold for sham rodents (Figure 9C, 1.14±0.13 g). When measuring the percent hypersensitivity relative to the uninjured paw, the spared nerve injury rodents exhibited a substantial increase in hypersensitivity relative to sham-treated rodents (Figure 9D, 87.1±2.5 vs. 3.3±1.8 %, respectively, $p<0.0001$). During the rescue phase rodents treated with V1-cal have a reduced hypersensitivity which markedly improved when compared to TAT_{47-57}-treated rodents (Figure 9D, 16.4±3.0 vs. 76.8±2.7 %, respectively, $p<0.0001$). As cold allodynia also has a robust response after spared

nerve injury, we repeated these studies in an additional group of mice while testing the response to acetone. V1-cal administration, as opposed to TAT_{47-57}, also rescued the licking and flinching behavior to acetone (Figure 9E).

Discussion

Here we identified a human TRPV1 genetic variant occurring just past the evolutionary conserved TRP box (residues 696-701) within the C-terminal TRP domain that alters the TRPV1-mediated response to noxious insults (10, 26). The CRISPR/Cas9-edited TRPV1^{K710N} knock-in mice provide evidence this TRPV1 variant reduces, yet does not completely abolish, TRPV1-mediated responses without changes in thermal response. Additionally, the reduced nociceptive response in TRPV1^{K710N} mice does not aggravate cellular injury but protects cells against noxious insults. As such, this study demonstrates a single amino acid variant in TRPV1 changes nociceptive behavior in rodents. Based on these findings, a TRPV1 peptide targeting the K710 region markedly reduces acute pain in addition to rescuing behavior after nerve injury.

Since the capsaicin receptor was cloned, the TRPV1 channel is recognized as a molecular integrator of noxious insults (27). Caterina MJ *et al.* reported that TRPV1 knockout mice were resistant to capsaicin-evoked behavior and a reduced response to noxious heat (28). Our results for the TRPV1^{K710N} knock-in mice identify that the TRPV1 channel can be modified by CRISPR/Cas9 to separate capsaicin-evoked behavior from the thermal response. In turn, this effect can be mimicked by a peptide targeting this TRPV1 region. Leaving the TRPV1-mediated thermal response intact is important as an increased thermal threshold could result in people inadvertently burning themselves (29). Additionally, TRPV1 antagonists such as AMG9810 can cause hyperthermia (30) which has hindered the development of an analgesic targeting TRPV1 (31). Here V1-cal limited TRPV1-mediated pain responses without causing hyperthermia. The results of our study suggest that a peptide-based approach to modulate the TRPV1 receptor avoids the complications seen with TRPV1 gene knockout or with administration of TRPV1 antagonists.

We also demonstrate that TRPV1^{K710N} knock-in mice have a reduced intensity of CGRP within DRG neurons. Prior literature identifies that CGRP release contributes to neurogenic inflammation (32) and capsaicin can increase CGRP levels in the DRG after injection (25). Further, isolated

mesenteric arteries of TRPV1 knockout mice release less CGRP with electric field stimulation(33). Our findings in TRPV1^{K710N} knock-in mice including a reduced paw thickness and blood flow response after capsaicin indicate that the TRPV1^{K710N} knock-in mice have less of a response to capsaicin-induced neurogenetic inflammation. Further, in isolated vessels, the TRPV1^{K710N} knock-in mice also have a decreased vasodilatory response to capsaicin. Since TRPV1 expressing sensory neurons induce neurogenic inflammation *via* the release of neuropeptides including SP and CGRP, leading to vasodilation and tissue edema (34), we also find that a peptide targeting this TRPV1 region, V1-cal, can also reduce these markers of neurogenic inflammation in wild type TRPV1 mice. Together, these findings identify that this TRPV1 missense variant leads to a reduced response in neurogenic inflammation.

Initial studies using TRPV1 knock-out rodents describe that TRPV1 was not involved in the mechanism of nerve injury-induced hypersensitivity (28, 35). However, TRPV1 knock-down by small interfering RNA (RNAi) or pharmacological inhibition reverses the mechanical hypersensitivity in a spinal nerve ligation mice model (36). This is opposed to the TRPV1 knockout rodents tested in the same study which exhibit similar behaviors in mechanical hypersensitivity relative to wild type rodents(36). In addition, the hypersensitivity caused by chronic constriction injury of the sciatic nerve could also be rescued by administration of siRNA targeting TRPV1 administered 7 days after injury or by the TRPV1 antagonist AMG-517 (37, 38). Prior literature indicate nerve injury-induced mechanical hypersensitivity is dependent on IB4^{+} neurons and independent of CGRP (39-42). In this context, the TRPV1^{K710N} mice, with a reduced baseline TRPV1 expression in IB4^{+} non-peptidergic neurons and attenuated nocifensive behaviors during nerve injury, could be attributed to the lower population of IB4^{+}/TRPV1^{+} DRG neurons relative to wild type TRPV1 mice. As the TRPV1 receptor remains functional for the TRPV1^{K710N} mice, this study provides further insight into the differences in results when using knockout TRPV1 mice as opposed to knockdown or pharmacological inhibition of TRPV1. We also found that V1-cal

attenuated cold allodynia in mice with spared nerve injury which could be due to TRPV1 directly regulating the response to TRPM8-mediated cold allodynia(43).

Acute or persistent pain behaviors are usually triggered by tissue or cellular injury, and the ability to detect noxious insults is essential to protect from further injury. As TRPV1 knockout mice exacerbate inflammation and injury post-ischemia (44, 45), it is important to highlight that the TRPV1^{K710N} mice could have a reduced pain behavior to insults without increasing cellular injury. In support of this, the TRPV1^{K710N} cardiomyocytes were resistant to both H_2O_2- and hypoxia-induced cell injury in addition to cerebral ischemia-reperfusion injury. Rapid production of ATP from glycolysis is crucial for the ischemic organs to meet energetic demand and neuronal activity under stress (46, 47). We found that the glycolytic capacity in primary adult cardiomyocytes from TRPV1^{K710N} mice was enhanced under stress. The enhancement of glycolysis during ischemia could reduce ischemic damage and improve cardiac function with reperfusion (48). Therefore, the enhanced glycolytic capacity in TRPV1^{K710N} cardiomyocytes might be beneficial to effectively provide energy and thus protect the cells against stress or ischemic insult.

The K710 site of TRPV1 is important in regulating TRPV1 function. Through site-directed mutagenesis, previous studies identified that K710 is a critical amino acid involving phosphatidylinositol 4,5-bisphosphate (PIP2) mediated TRPV1 activation (49). Moreover, the K710 site can be directly bound by LPA, a phospholipid that is important in the generation and maintenance of pain (19, 50). K710 is a positively charged residue within the C-terminal TRP domain of the TRPV1 channel, and the charged amino acid is important in stabilizing the α-helix (51). We found that the K710N mutation in rat TRPV1, which introduces a neutrally charged amino acid residue, markedly reduces calcium influx evoked by capsaicin, suggesting the importance of K710 in capsaicin-induced TRPV1 gating. The *in vitro* data was further verified in the CRISPR/Cas9-edited TRPV1^{K710N} knock-in mice. A previous study revealed that substitution of K710 with a neutrally or negatively charged amino acid caused a marked decrease in TRPV1

current evoked by LPA in HEK293 cells but did not alter the response to capsaicin (19). Consistent with that data, our results show that TRPV1^{K710N} mice were resistant to acute pain induced by the LPA analog Brp-LPA that can induce pain by directly activating TRPV1 independent of LPA receptors (19). However, unlike the previous study, responses to capsaicin were also impaired due to the K710N mutation in cells and rodents. These findings suggest that capsaicin-induced TRPV1 activation is determined not only by the critical binding site of Y511 located in the region linking the second and third transmembrane segments that was previously described (13), but also by the K710 in the C-terminal TRP domain that contributes to the channel gating.

Although CRISPR/Cas9-based technology allows researchers to effectively edit single or multiple genes *in vitro* and *in vivo*, there are still concerns regarding safety and ethics such as off-target effects or undesirable side-effects. In this study, we did not perform whole genome sequencing on the TRPV1^{K710N} mice to rule out the possibility of off-target mutations. However, we used pronuclear microinjection method to directly deliver the Cas9 protein and gRNA, which could largely reduce the off-target effects (52). Moreover, off-target mutations are rare in Cas9-edited mice (53), and we also initially backcrossed the TRPV1^{K710N} mice with wild type C57BL/6 mice to further remove potential inter-chromosomal off-target mutations. Although TRPV1 is well established for a role in pain transmission and thermoregulation, several reports indicate TRPV1 is also broadly distributed within the brain and potentially involved in memory and motor function (54-56). Considered within the context of our testing, the TRPV1^{K710N} mice had normal appearance, fertility and motor function suggesting the K710N genetic variant did not have any profound impact on brain function. As our behavioral assays were mainly reflex or spontaneous assays, our results are potentially limited as we did not assess operant or pain-affected complex behaviors. Further, we only assessed hypersensitivity and did not assess spontaneous pain or non-reflexive withdrawal in our nerve injury studies. We also used Fura-2 changes in calcium influx to assess TRPV1 function however, did not use patch clamping to investigate how the K710N TRPV1 variant affects

TRPV1 function. A prior report using patch clamped endothelial cells does describe how acute administration of V1-cal can block 12-HETE-induced activation of TRPV1 (15). We also did not use TRPV1 knockout mice to determine whether there are off-target effects of the V1-cal peptide for a spared nerve injury model. However, a prior study using TRPV1 knockout rats in a cardiovascular model showed that V1-cal selectively targets TRPV1(23). Further, although the K710N variant is reported at a low frequency in humans (1.645×10^{-5} frequency), no pathophysiology related to this point mutation have been described (gnomAD ID:17-3475514-C-A).

In summary, we generated a CRISPR/Cas9-edited TRPV1^{K710N} mouse based upon a human missense variant within the TRPV1 TRP domain that results in human TRPV1 to have avian-like TRPV1 qualities. The avian-like TRPV1^{K710N} mice provide evidence that K710 site in the C-terminus of mammalian TRPV1 is critical for channel gating and nociception. Our data suggest that mitigating, yet not eliminating, TRPV1-mediated response to noxious stimuli can limit pain behaviors while reducing cellular injury. A peptide targeted the region spanning the K710 residue further provides a non-opioid therapeutic by targeting a genetically divergent region between avian and mammalian species to limit pain transmission.

Methods

GnomAD database analysis

The single-nucleotide variants of the *TRPV1* transcript (ENSG00000196689.6) were accessed from Genome Aggeration Database (gnomAD, Version 2.1.1). Synonymous single-nucleotide variants within the 3' and 5' UTRs or introns were filtered to include only missense variants and predicted loss-of -function variants for analysis. The human TRPV1 missense variants and predicted loss-of -function variants were then compared with genetic divergent residues in avian TRPV1 sequences to determine variants which cause a divergence of human TRPV1 to avian TRPV1.

In silico structural analysis

To investigate these identified variants further, we performed *in silico* analysis based on the published crystal structure of closed-state rat TRPV1 (PDB ID: 3J5P) (10). Further, we focused on the TRP domain and the substitution of Thr>Ile 708 (T708I) or Lys>Asn 710 (K710N) was individually introduced into the TRPV1 monomer structure model using UCSF Chimera program (57). The rotamer with the highest probability was applied followed by 100 cycles of energy minimization. PyMOL (PyMOL Molecular Graphics System, Version 2.0 Schrödinger, LLC.) was used to visualize the resulting structure models and check the loss or gain of polar interactions between neighboring residues located adjacent to the mutation.

Rodent Studies

All animal experiments followed the Animal Research: Reporting of *In Vivo* Experiments (ARRIVE) guidelines (58). Animals were housed under standard conditions of temperature (21±2°C) and humidity (55±5%), with food and water *ad libitum* in a 12:12 hours day/night cycle. The wild type TRPV1 and TRPV1^{K710N} animals were allocated to experimental groups by age-matching and researchers were blinded to the genotype of the mice when conducting animal experiments and analyzing the data.

Generation of CRISPR/Cas9 edited TRPV1^{K710N} knock-in mice

The CRISPR/Cas9 gene-editing procedures were performed in Transgenic, Knockout and Tumor model Center (TKTC) at Stanford University. TRPV1^{K710N} mice were generated by introducing a mixture of gRNA (15 ng/μl), donor oligo DNA (5 ng/μl) and Cas9 protein (30 ng/μl) by pronuclear microinjection into C57BL/6 mouse zygotes. Over 100 zygotes were injected and implanted into surrogate mothers' oviducts. A total of 16 pups were born, and genomic DNA was extracted from tail biopsies followed by PCR amplification using a specific primer set to identify founders (F0). The PCR products were subjected to T7EI cleavage assay to confirm Cas9-mediated on-target cleavage of TRPV1. DNA sequencing analysis was used to further determine the mouse genotype. The correctly integrated mutant F0 mice were further back-crossed with wild type C57BL/6J mice to produce offspring (F1) followed by intercrossing for two additional generations to obtain TRPV1^{K710N} homozygotes. Sequence information of gRNA, ssODN, and primers are provided (Supplemental Table S2).

Capsaicin-laced food test

Wild type TRPV1 and TRPV1^{K710N} C57BL/6 mice at 10-20 weeks of age, both male and female, were used. On the day of testing, five mice of each group were placed into a clean mouse cage (no bedding inside). The same amount (10g) of capsaicin-free bird food (Deck, Porch N' Patio, Wild Delight) was put on the cage bottom and the behavior response were recorded by a video. Seven days after this test, the same mice were administered capsaicin-laced bird food (10g, Sizzle N' Heat, Wild Delight). For a 10 min period, defensive withdrawal behavior, defined as at least three paws climbing on the cage wall or jumping, was counted by an observer blinded to the genotype of the mice.

Behavioral testing

The behavioral experiments were conducted between 9 am and 4 pm and were in accordance with the ethical guidelines of the International Association for the Study of Pain (59). Wild type TRPV1 and TRPV1^{K710N} mice at 10-20 weeks of age, both male and female, were acclimated to this

environment for 15 min prior to starting the experiment. The doses of capsaicin and Brp-LPA used to trigger pain behaviors in this study were based on prior literature(19, 60). Capsaicin (1.5µg/paw in 20µL, Sigma-Aldrich), Brp-LPA (4.1µg/paw in 20µL, Echelon Biosciences) or the corresponding vehicle (0.25% ethanol in saline or saline alone, respectively) were administered intraplantarly. Further, the V1-cal peptide (1µg/paw in 20µL, Genscript), or $TAT_{47\text{-}57}$ (1µg/paw in 20µL, Genscript) was administrated intraplantarly 15 minutes before capsaicin or Brp-LPA injection. Immediately after injection, nociceptive behavior (paw-licking and flinching) was quantified for 5 min immediately after injection (19, 61). Paw thickness was also measured 20 min after capsaicin injection using a digital caliper placed near the injection site. Each measurement was repeated three times. The observer was blinded to the mouse genotype.

Laser-Doppler blood flow measurement

Rodents were anesthetized with isoflurane (2%) and placed on a temperature-controlled heating pad to maintain body temperature within a normal range (37-38°C). Blood flow in the plantar skin was monitored by a laser Doppler Flowmeter (Perimed, Sweden, assessed as arbitrary units) with a flexible fiber optic probe gently fixed to the paw injected with capsaicin (1.5µg/paw in 20µL) or vehicle (ethanol in saline, 20 µL). The baseline blood flow was measured for 10 min and continued to monitor the blood flow for 20 min after capsaicin injection.

Temperature measurements

Rectal Temperature: To examine the effects of peptides and AMG9810 on temperature, V1-Cal (1mg/kg), $TAT_{47\text{-}57}$ (1mg/kg), AMG9810 (30mg/kg, Alomone labs, Israel), or the corresponding vehicle (saline for peptides and 5% ethanol in saline for AMG9810) were intraperitoneally injected. The doses of peptides and AMG9810 were based on prior literature(23, 62). The rectal temperature was measured at 10-min intervals for a total of 90 min after the administration of drugs. The rectal temperature of the mice was measured with a rectal thermal probe (diameter 1.5 mm) connected to

a digital thermometer (Ruiwode, China) with the rectal probe was inserted to a depth of 1.5 cm for at least 10 sec. The measurement was performed at room temperature of 24.0 °C.

Body Temperature: Mice were housed for the duration of the testing in a temperature-controlled animal housing facility monitored and maintained at a temperature of 22±0.4°C at Stanford University. A temperature probe (14x2.2mm,120mg, IPTT-300 Temperature Transponder, Bio Medic Data Systems) was implanted subcutaneously dorsal and lateral to the L1-L4 region of the mouse with a reported accuracy of ±0.6°C (63). After three days, body temperatures were measured in the morning and afternoon using a scanner (DAS-8007IUS Reader, Bio Medic Data Systems) that allowed for temperature measurements in conscious mice in home cages.

Pressure Myography

Third-order mesenteric arteries of wild type TRPV1 or TRPV1^{K710N} mice were dissected under the microscope and remaining fat was removed. Arteries were mounted on cannulas in a vessel chamber (Living Systems Instrumentation). The chamber was filled with calcium-buffer and a pressure of 80mmHg was applied to each vessel. After generation of myogenic tone 10nM (R)-phenylephrine hydrochloride (Phe) was added for preconstriction. After preconstriction, increasing concentrations of capsaicin (10^{-9} to 10^{-4} M) were added in intervals of 1 minute and relaxation response was measured using digital video edge-detection. In a separate series of experiments, wild type TRPV1 arteries were perfused with 1μM V1-cal or TAT_{47-57} for 3min before increasing concentrations of capsaicin were given.

Immunohistochemistry

Mice were euthanatized and perfused intracardially with phosphate buffered saline (PBS) followed by 4% buffered paraformaldehyde. Subsequently, the DRGs at L4-L5 segments were removed and fixed in 4% buffered paraformaldehyde for 24 h followed by immersion in 30% sucrose overnight. The tissue samples were embedded in OCT compound and cryostat sections (10μm) were prepared in a cryostat (NX50, ThermoFisher, USA) at -20°C. The sections were blocked and then incubated

with the following primary antibodies: mouse anti-TRPV1 (75-254, NeuroMab, USA), rabbit anti-CGRP (14959, CST, USA) or guinea pig anti-SP (GP14110, Neuromics, USA) at 4 °C overnight. After incubation with primary antibodies, the sections were washed with PBS and then incubated with Alexa Fluor 488 or 594 conjugated secondary antibodies (Invitrogen, USA) at 37 °C for 1 h. For IB4 staining, DRG sections were incubated with Isolectin B4 (BSI-B4), FITC conjugate (L2895, Sigma, USA) at room temperature for 2h. Sections were washed in PBS, mounted in anti-fade mounting medium with DAPI (Invitrogen, USA), and imaged under a fluorescence microscope (Zeiss, Germany) followed by analysis of the fluorescence intensity with Image J 1.51s (NIH).

Glycolysis stress test

A glycolysis stress test was conducted using the Seahorse extracellular flux analyzer (XFp Seahorse Bioscience) following the manufacturer's instructions. Adult cardiac myocytes of wild type TRPV1 or TRPV1^{K710N} mice were seeded in an 8-well laminin pre-coated miniplate at a density of 1000 cells/well. After culturing overnight, the cells were washed twice using a Seahorse XF Base Medium without glucose and pyruvate and supplemented with 2 mM glutamine (pH7.4). Glucose (5.5mM) was injected to induce glycolytic response, oligomycin (2 μM) was injected to inhibit mitochondrial ATP production, and 2-DG (50mM) to inhibit glycolysis through competitively binding to glucose hexokinase. The real-time ECAR was directly measured to assess the key parameters of glycolytic function: glycolysis, glycolytic capacity, glycolytic reserve, and non-glycolytic acidification.

Spared Nerve Injury (SNI) Model

Wild type C57BL/6J or TRPV1^{K710N} male mice (10-16 weeks of age) were anesthetized with isoflurane (1-3%) and placed on a heating pad to maintain body temperature (37°C). The left hindleg was prepared and a longitudinal incision (~1cm) made in the skin proximal to the knee. Under a stereomicroscope, the muscle layer was blunt dissected to reveal the common peroneal, tibial, and sural branches of the sciatic nerve. Leaving the sural nerve undisturbed, ~2mm of the

common peroneal and tibial nerves were transected and removed. The skin incision was then closed with silk suture, and mice closely monitored during recovery. For the sham surgery, the common peroneal, tibial, and sural branches of the sciatic nerve were located but left undisturbed.

Osmotic pump implantation and drug delivery

For Alzet osmotic pump implantation (volume 100μL, Alzet model no. 1002, USA), an incision was made at the nape of the mouse neck and the pump implanted immediately below the skin layer and closed with silk suture for subcutaneous continuous delivery of the V1-cal peptide (1.0 mg/kg/day), or TAT_{47-57} (1.0 mg/kg/day) for two weeks from day 14 to day 28 post SNI surgery. Pumps were filled and then primed in 0.9% sterile saline at 37°C for ~24 hours prior to implantation.

Mechanical and thermal nociception assessments

Mechanical, thermal and cold nociceptive behaviors were assessed in mice subjected to SNI or sham operation during baseline, post-SNI or sham, and post-treatment stages of the protocol.

To assess mechanical nociception, mice were placed individually in a plexi-glass chamber on an elevated mesh screen stand and allowed to acclimate for a minimum of 10 minutes. The up-down technique was performed before (baseline) and after SNI or sham operation (64, 65). von Frey fibers ranging in force from 0.004 to 5.49g were applied perpendicularly to the mouse hind paw lateral surface until the paw was withdrawn. Once a response was identified, the next lower von Frey hair was applied. For each positive response (paw withdrawal), the next lesser filament was tested. For each negative response, the next higher filament was tested. The sequence of positive and negative responses was recorded and incorporated in an established curve-fitting algorithm to determine mechanical sensitivity (66).

To assess for changes in thermal nociception, Hargreaves method was used to determine hind paw withdrawal threshold. Mice were placed individually in plexi-glass chambers on a glass platform and allowed to acclimate for 10 minutes. The heat stimulus from a focused heat light source using a commercial Plantar Test Analgesia Meter (IITC Life Science) was applied to the ventral lateral

surface of the hind paw with a light intensity of 30% determined in preliminary trials. Reaction time was measured in 0.01 second increments with a cut off time of 15 seconds to prevent thermal damage to the paw region. A minimum of 30 seconds separated testing of the hind paws (67).

To assess acetone-induced cold nociception, 50 μL of acetone solution was applied onto the lateral plantar surface of the paw, using a blunt needle connected to a syringe without touching the skin. The duration of the nociceptive response of paw licking and flinching was recorded for 60 sec.(68, 69)

Statistical analysis

Based upon an *a priori* power analysis, we calculated that a minimum of 6 rodents were necessary to achieve at least a 20% minimal difference in behavioral responses and a minimum of 3 experimental replicates for non-behavioral assays for a power of 80 % and α=0.05. Data are expressed as mean ±SEM. Results were analyzed using GraphPad Prism 8.0 (GraphPad Software Inc.). Unpaired two tailed or one tailed *t*-test was used for comparisons between two experimental groups. Comparisons among multiple groups were conducted *via* one-way or two-way analysis of variance (ANOVA) followed by *post hoc* Tukey's test or Bonferroni test or when groups were uneven, a mixed-effects analysis model was used. Statistical significance was set at $p<0.05$.

Study approval

All animal studies conformed to the National Institute of Health Guide for the Care and Use of Laboratory Animals (NIH Publications No. 85-23 revised in 1996). All animal studies have been approved by the appropriate ethics committee (Stanford University, Anhui Medical University, Butantan Institute, and University of Munster) and performed in accordance with the ethical standards laid down in the 1964 Declaration of Helsinki and its later amendments.

Author Contributions:

ERG, SFH, SLM, NMW and PS conceived and designed the experiments. SFH, VOZ, PS, YB, FR, LB, RCH, BH, XY, MZ, BS, ZFL, CW, SLM and LJX performed the experiments and analyzed the data. SFH and ERG wrote the manuscript, which was revised by VOZ, PS, KJS, CMS, and YZ.

Acknowledgments

We would like to thank Dr. Hong Zeng and Dr. Zhuanfen Cheng in Transgenic, Knockout and Tumor model Center (TKTC) at Stanford University for assistance with generating the TRPV1^{K710N} knock-in mice. **Funding:** This work was supported by NIH NIGMS GM119522 and GM119522S01 along with a Stanford Cardiovascular Institute seed grant (E.R. Gross), National Natural Science of Foundation of China No. 32271194, the State Scholarship Fund of China Scholarship Council No.201708340038 and the Second Hospital of Anhui medical University seed grant No. 2019GMFY01 (S. He), São Paulo Research Foundation (FAPESP) 2018/19332-7 (V.O. Zambelli), Coodernacão de Aperfeiçoamento de Pessoal de Nível Superior-Brasil (CAPES), Finance Code 001 (B. Stein), NIH grant T32 GM089626 (S.L. McAllister), Stanford Diabetes Research Center P30DK116074 and DK125260 (K Svensson), American Heart Association (AHA) postdoctoral fellowship #905674 (M Zhao), and German Research Foundation / Deutsche Forschungsgemeinschaft DFG, WA3786/2-1(N.M. Wagner).

References

1. Gaskin DJ, Richard P. The economic costs of pain in the United States. *J Pain.* 2012;13(8):715-24.
2. Manchikanti L, et al. COVID-19 and the Opioid Epidemic: Two Public Health Emergencies That Intersect With Chronic Pain. *Pain Ther.* 2021.
3. Cox JJ, et al. An SCN9A channelopathy causes congenital inability to experience pain. *Nature.* 2006;444(7121):894-8.
4. Yang Y, et al. Mutations in SCN9A, encoding a sodium channel alpha subunit, in patients with primary erythermalgia. *J Med Genet.* 2004;41(3):171-4.
5. Fertleman CR, et al. SCN9A mutations in paroxysmal extreme pain disorder: allelic variants underlie distinct channel defects and phenotypes. *Neuron.* 2006;52(5):767-74.
6. Caterina MJ, et al. The capsaicin receptor: a heat-activated ion channel in the pain pathway. *Nature.* 1997;389(6653):816-24.
7. Moran MM, Szallasi A. Targeting nociceptive transient receptor potential channels to treat chronic pain: current state of the field. *British journal of pharmacology.* 2018;175(12):2185-203.
8. Ryu S, et al. Uncoupling proton activation of vanilloid receptor TRPV1. *The Journal of neuroscience : the official journal of the Society for Neuroscience.* 2007;27(47):12797-807.
9. Nilius B, Szallasi A. Transient receptor potential channels as drug targets: from the science of basic research to the art of medicine. *Pharmacological reviews.* 2014;66(3):676-814.
10. Liao M, et al. Structure of the TRPV1 ion channel determined by electron cryo-microscopy. *Nature.* 2013;504(7478):107-12.

11. Moreno AM, et al. Long-lasting analgesia via targeted in situ repression of NaV1.7 in mice. *Sci Transl Med.* 2021;13(584).

12. Remmel A. CRISPR-based gene therapy dampens pain in mice. *Nature.* 2021;591(7850):359.

13. Jordt SE, Julius D. Molecular basis for species-specific sensitivity to "hot" chili peppers. *Cell.* 2002;108(3):421-30.

14. Stambaugh K, et al. Additive effects of late preconditioning produced by monophosphoryl lipid A and the early preconditioning mediated by adenosine receptors and KATP channel. *Circulation.* 1999;99(25):3300-7.

15. Otto M, et al. 12(S)-HETE mediates diabetes-induced endothelial dysfunction by activating intracellular endothelial cell TRPV1. *J Clin Invest.* 2020;130(9):4999-5010.

16. Deng F, et al. The gut microbiota metabolite capsiate promotes Gpx4 expression by activating TRPV1 to inhibit intestinal ischemia reperfusion-induced ferroptosis. *Gut Microbes.* 2021;13(1):1-21.

17. Gregorio-Teruel L, et al. The Integrity of the TRP Domain Is Pivotal for Correct TRPV1 Channel Gating. *Biophys J.* 2015;109(3):529-41.

18. Paquet D, et al. Efficient introduction of specific homozygous and heterozygous mutations using CRISPR/Cas9. *Nature.* 2016;533(7601):125-9.

19. Nieto-Posadas A, et al. Lysophosphatidic acid directly activates TRPV1 through a C-terminal binding site. *Nature chemical biology.* 2011;8(1):78-85.

20. Lin Q, et al. Roles of TRPV1 and neuropeptidergic receptors in dorsal root reflex-mediated neurogenic inflammation induced by intradermal injection of capsaicin. *Mol Pain.* 2007;3:30.

21. Bourquin AF, et al. Assessment and analysis of mechanical allodynia-like behavior induced by spared nerve injury (SNI) in the mouse. *Pain.* 2006;122(1-2):14 e1-.

22. Pei Z, et al. alpha,beta-Unsaturated aldehyde crotonaldehyde triggers cardiomyocyte contractile dysfunction: role of TRPV1 and mitochondrial function. *Pharmacological research.* 2014;82:40-50.

23. Hurt CM, et al. Transient Receptor Potential Vanilloid 1 Regulates Mitochondrial Membrane Potential and Myocardial Reperfusion Injury. *Journal of the American Heart Association.* 2016;5(9):e003774.

24. Wang Y, et al. TRPV1 agonism inhibits endothelial cell inflammation via activation of eNOS/NO pathway. *Atherosclerosis.* 2017;260:13-9.

25. Li D, et al. Sensitization of primary afferent nociceptors induced by intradermal capsaicin involves the peripheral release of calcitonin gene-related Peptide driven by dorsal root reflexes. *J Pain.* 2008;9(12):1155-68.

26. Valente P, et al. Identification of molecular determinants of channel gating in the transient receptor potential box of vanilloid receptor I. *FASEB journal : official publication of the Federation of American Societies for Experimental Biology.* 2008;22(9):3298-309.

27. Tominaga M, et al. The cloned capsaicin receptor integrates multiple pain-producing stimuli. *Neuron.* 1998;21(3):531-43.

28. Caterina MJ, et al. Impaired nociception and pain sensation in mice lacking the capsaicin receptor. *Science.* 2000;288(5464):306-13.

29. Garami A, et al. TRPV1 antagonists that cause hypothermia, instead of hyperthermia, in rodents: Compounds' pharmacological profiles, in vivo targets, thermoeffectors recruited and implications for drug development. *Acta physiologica.* 2018;223(3):e13038.

30. Gavva NR, et al. The vanilloid receptor TRPV1 is tonically activated in vivo and involved in body temperature regulation. *The Journal of neuroscience : the official journal of the Society for Neuroscience.* 2007;27(13):3366-74.

31. Garami A, et al. Hyperthermia induced by transient receptor potential vanilloid-1 (TRPV1) antagonists in human clinical trials: Insights from mathematical modeling and meta-analysis. *Pharmacology & therapeutics.* 2020;208:107474.

32. Brain SD, et al. Calcitonin gene-related peptide is a potent vasodilator. *Nature.* 1985;313(5997):54-6.

33. Wang LH, et al. Impaired vasodilation in response to perivascular nerve stimulation in mesenteric arteries of TRPV1-null mutant mice. *J Hypertens.* 2006;24(12):2399-408.

34. Chiu IM, et al. Neurogenic inflammation and the peripheral nervous system in host defense and immunopathology. *Nat Neurosci.* 2012;15(8):1063-7.

35. Bolcskei K, et al. Investigation of the role of TRPV1 receptors in acute and chronic nociceptive processes using gene-deficient mice. *Pain.* 2005;117(3):368-76.

36. Christoph T, et al. Investigation of TRPV1 loss-of-function phenotypes in transgenic shRNA expressing and knockout mice. *Mol Cell Neurosci.* 2008;37(3):579-89.

37. Guo SH, et al. Silencing of spinal Trpv1 attenuates neuropathic pain in rats by inhibiting CAMKII expression and ERK2 phosphorylation. *Scientific reports.* 2019;9(1):2769.

38. Bai J, et al. Attenuation of TRPV1 by AMG-517 after nerve injury promotes peripheral axonal regeneration in rats. *Molecular pain.* 2018;14:1744806918777614.

39. Tarpley JW, et al. The behavioral and neuroanatomical effects of IB4-saporin treatment in rat models of nociceptive and neuropathic pain. *Brain Res.* 2004;1029(1):65-76.

40. Pinto LG, et al. Non-Peptidergic Nociceptive Neurons Are Essential for Mechanical Inflammatory Hypersensitivity in Mice. *Mol Neurobiol.* 2019;56(8):5715-28.

41. Barabas ME, Stucky CL. TRPV1, but not TRPA1, in primary sensory neurons contributes to cutaneous incision-mediated hypersensitivity. *Molecular pain.* 2013;9:9.

42. Ishida K, et al. Calcitonin gene-related peptide is not involved in neuropathic pain induced by partial sciatic nerve ligation in mice. *Neurosci Lett.* 2022;778:136615.

43. Li F, et al. TRPV1 activity and substance P release are required for corneal cold nociception. *Nature communications.* 2019;10(1):5678.

44. Zhong B, et al. Knockout of TRPV1 Exacerbates Ischemia-reperfusion-induced Renal Inflammation and Injury in Obese Mice. *In Vivo.* 2020;34(5):2259-68.

45. Wang L, Wang DH. TRPV1 gene knockout impairs postischemic recovery in isolated perfused heart in mice. *Circulation.* 2005;112(23):3617-23.

46. Jang S, et al. Glycolytic Enzymes Localize to Synapses under Energy Stress to Support Synaptic Function. *Neuron.* 2016;90(2):278-91.

47. Koronowski KB, et al. Neuronal SIRT1 (Silent Information Regulator 2 Homologue 1) Regulates Glycolysis and Mediates Resveratrol-Induced Ischemic Tolerance. *Stroke.* 2017;48(11):3117-25.

48. Oeing CU, et al. MTORC1-Regulated Metabolism Controlled by TSC2 Limits Cardiac Reperfusion Injury. *Circ Res.* 2021.

49. Brauchi S, et al. Dissection of the components for PIP2 activation and thermosensation in TRP channels. *Proceedings of the National Academy of Sciences of the United States of America.* 2007;104(24):10246-51.

50. Ueda H. Pathogenic mechanisms of lipid mediator lysophosphatidic acid in chronic pain. *Progress in lipid research.* 2021;81:101079.

51. Richardson JS, Richardson DC. Amino acid preferences for specific locations at the ends of alpha helices. *Science.* 1988;240(4859):1648-52.

52. Wang HX, et al. CRISPR/Cas9-Based Genome Editing for Disease Modeling and Therapy: Challenges and Opportunities for Nonviral Delivery. *Chem Rev.* 2017;117(15):9874-906.

53. Iyer V, et al. Off-target mutations are rare in Cas9-modified mice. *Nat Methods.* 2015;12(6):479.

54. Cavanaugh DJ, et al. Trpv1 reporter mice reveal highly restricted brain distribution and functional expression in arteriolar smooth muscle cells. *The Journal of neuroscience : the official journal of the Society for Neuroscience.* 2011;31(13):5067-77.

55. Marsch R, et al. Reduced anxiety, conditioned fear, and hippocampal long-term potentiation in transient receptor potential vanilloid type 1 receptor-deficient mice. *The Journal of neuroscience : the official journal of the Society for Neuroscience.* 2007;27(4):832-9.

56. Dawbarn D, et al. Intranigral injection of capsaicin enhances motor activity and depletes nigral 5-hydroxytryptamine but not substance P. *Neuropharmacology.* 1981;20(4):341-6.

57. Pettersen EF, et al. UCSF Chimera--a visualization system for exploratory research and analysis. *J Comput Chem.* 2004;25(13):1605-12.

58. Kilkenny C, et al. Improving bioscience research reporting: the ARRIVE guidelines for reporting animal research. *PLoS Biol.* 2010;8(6):e1000412.

59. Zimmermann M. Ethical guidelines for investigations of experimental pain in conscious animals. *Pain.* 1983;16(2):109-10.

60. Scherrer G, et al. VGLUT2 expression in primary afferent neurons is essential for normal acute pain and injury-induced heat hypersensitivity. *Proceedings of the National Academy of Sciences of the United States of America.* 2010;107(51):22296-301.

61. Pereira GJV, et al. Capsaicin-like analogue induced selective apoptosis in A2058 melanoma cells: Design, synthesis and molecular modeling. *Bioorg Med Chem.* 2019;27(13):2893-904.

62. Andreev YA, et al. Polypeptide modulators of TRPV1 produce analgesia without hyperthermia. *Mar Drugs.* 2013;11(12):5100-15.

63. Wacker CB, et al. The use of small subcutaneous transponders for quantifying thermal biology and torpor in small mammals. *Journal of thermal biology.* 2012;37(4):250-4.

64. Chaplan SR, et al. Quantitative assessment of tactile allodynia in the rat paw. *J Neurosci Methods.* 1994;53(1):55-63.

65. Dixon WJ. Staircase bioassay: the up-and-down method. *Neurosci Biobehav Rev.* 1991;15(1):47-50.

66. Zambelli VO, et al. Aldehyde dehydrogenase-2 regulates nociception in rodent models of acute inflammatory pain. *Sci Transl Med.* 2014;6(251):251ra118.

67. McAllister SL, et al. Aberrant reactive aldehyde detoxification by aldehyde dehydrogenase-2 influences endometriosis development and pain-associated behaviors. *Pain.* 2021;162(1):71-83.

68. Decosterd I, Woolf CJ. Spared nerve injury: an animal model of persistent peripheral neuropathic pain. *Pain.* 2000;87(2):149-58.

69. Zhang MD, et al. Ca2+-binding protein NECAB2 facilitates inflammatory pain hypersensitivity. *J Clin Invest.* 2018;128(9):3757-68.

Figures and Figure legends

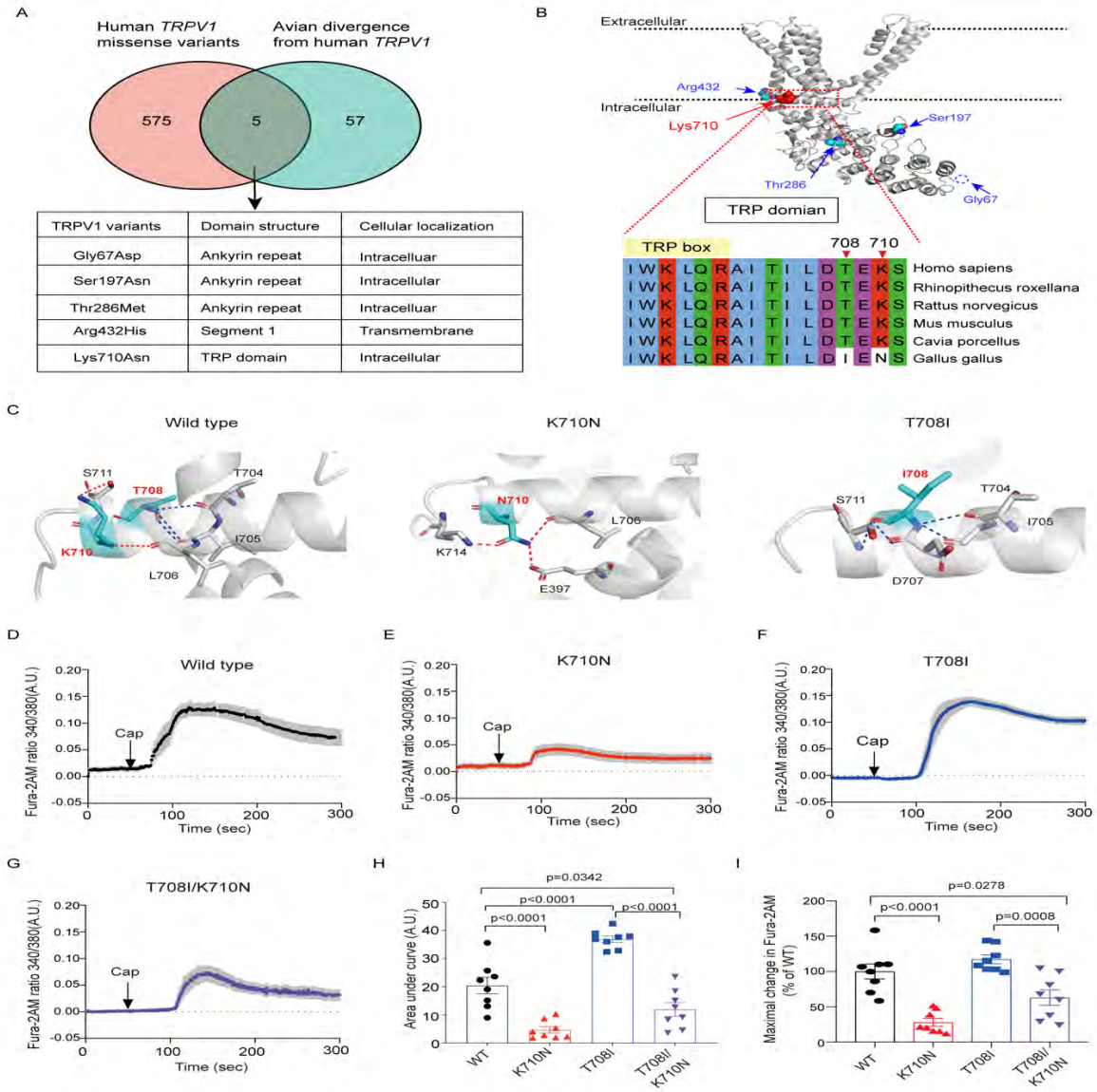

Figure 1 Identification of a human missense TRPV1 variant that reduces TRPV1-mediated calcium influx. (A) Venn diagram identifying 5 missense TRPV1 variants that intersect when examining the human TRPV1 missense variants from gnomAD and avian genetic divergence from the human TRPV1 sequence. (B) Location of these 5 missense variants within the rat TRPV1 structure (PDB ID:3J5P). Alignment of the mammalian and avian TRP domain (I696-S711 within the red dotted box and the un-conserved amino acids, 708 and 710 in white). (C) 3D structure of wild type TRPV1, K710N and T708I, based on the closed-state rat TRPV1 molecular model (PDB ID: 3J5P). Polar contacts are indicated as red or blue dashed lines. (D-G) Calcium influx in response to 1μM capsaicin (Cap) with (D) wild type TRPV1, (E) K710N, (F) T708I or (G) K710N/T708I TRPV1 mutations presented as Fura-2 AM ratio 340/380 nm. (H) The area under curve (AUC, total amount of calcium influx) and (I) the percent maximal change in Fura-2 ratio for TRPV1 mutants relative to wild type TRPV1 were calculated. n=8 cells/group from three independent experiments. Data are expressed as mean±SEM. One-way ANOVA followed by Tukey's *post hoc* test.

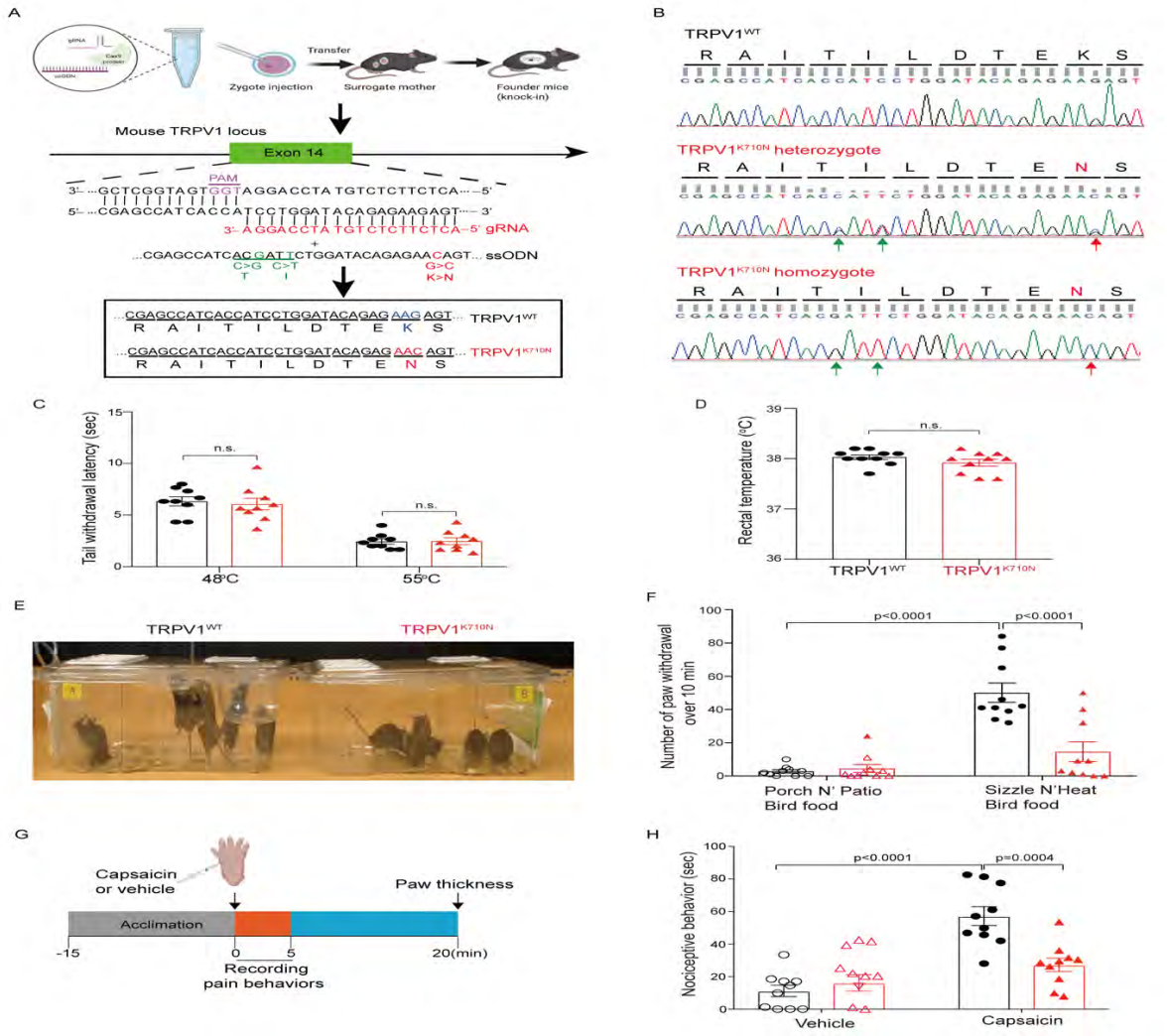

Figure 2 Construction of CRISPR/Cas-9 edited TRPV1^{K710N} knock-in mice followed by thermal and behavioral testing. (A) Schematic diagram for generation of CRISPR/Cas-9 edited TRPV1^{K710N} knock-in mice. Design of gRNA, ssODNs lead to the K710N mutation (red) and two silent mutations (green) in the protospacer adjacent motif (PAM, purple). (B) Representative DNA sequencing for wild type (WT) TRPV1, TRPV1^{K710N} heterozygotes (double peaks), or TRPV1^{K710N} homozygotes (single peak). Red arrow: the designed mutation; Green arrow: silent mutations. (C) Tail withdrawal latency time (sec) in response to hot water at 48^{O}C and 55^{O}C n=9/group. (D) Body temperature detected by a rectal temperature probe in wild type TRPV1 and homozygous TRPV1^{K710N} mice, n=10/group. (E) Representative image showing the difference in response to stepping on capsaicin-laced food for wild type TRPV1 and TRPV1^{K710N} mice. (F) Paw withdrawal behavior for wild type TRPV1 and TRPV1^{K710N} mice exposed to capsaicin-laced bird food (Sizzle N' Heat Bird food) or regular bird food (Porch N' Patio Bird food), n=10/group. (G) Experimental protocol for nociceptive behavior by intraplantar capsaicin injection in wild type TRPV1 and TRPV1^{K710N} mice. (H) Nociceptive behavior (paw-licking/flicking) n=10/group. Data are expressed as mean ± SEM. Black dot: wild type TRPV1 mice; Red triangle: homozygous TRPV1^{K710N} mice. Hollow: vehicle treatment, solid: capsaicin treatment. For (C, D) determined by unpaired t-test and (F, H), two-way ANOVA followed by Tukey's *post hoc* test.

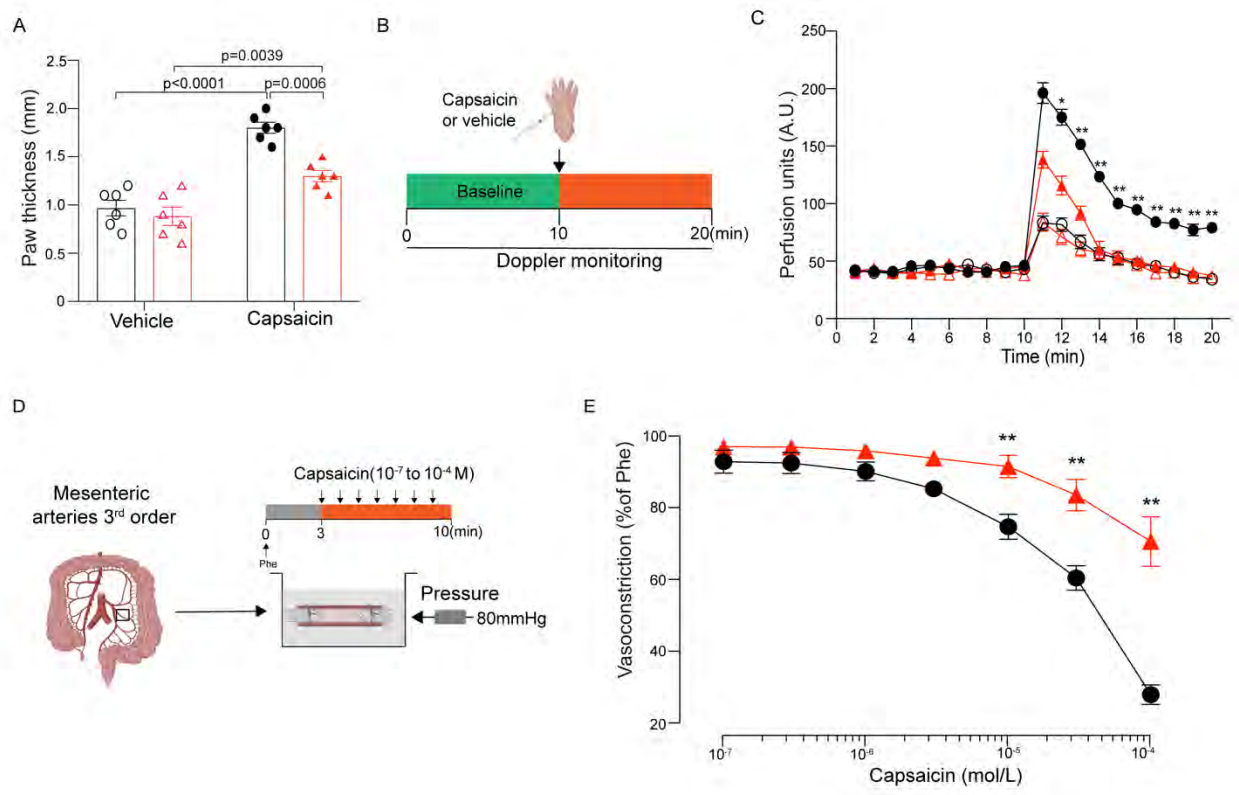

Figure 3 Vascular response in TRPV1^{K710N} knock-in mice. (A) Paw thickness and (B, C) blood flow induced by paw injection of capsaicin or vehicle for wild type TRPV1 and TRPV1^{K710N} mice. n=6/group (D, E) Pressure myography showing vascular response to capsaicin in wild type TRPV1 (n=7) and TRPV1^{K710N} mice (n=8). Data are expressed as mean ± SEM. In (C, E), two-way RM ANOVA followed by Bonferroni's *post hoc* test with *p<0.05, **p<0.01, capsaicin group of wild type TRPV1 mice *vs.* capsaicin group of TRPV1^{K710N} mice. Black dot: wild type TRPV1 mice; Red triangle: homozygous TRPV1^{K710N} mice. Phe= (R)-phenylephrine hydrochloride.

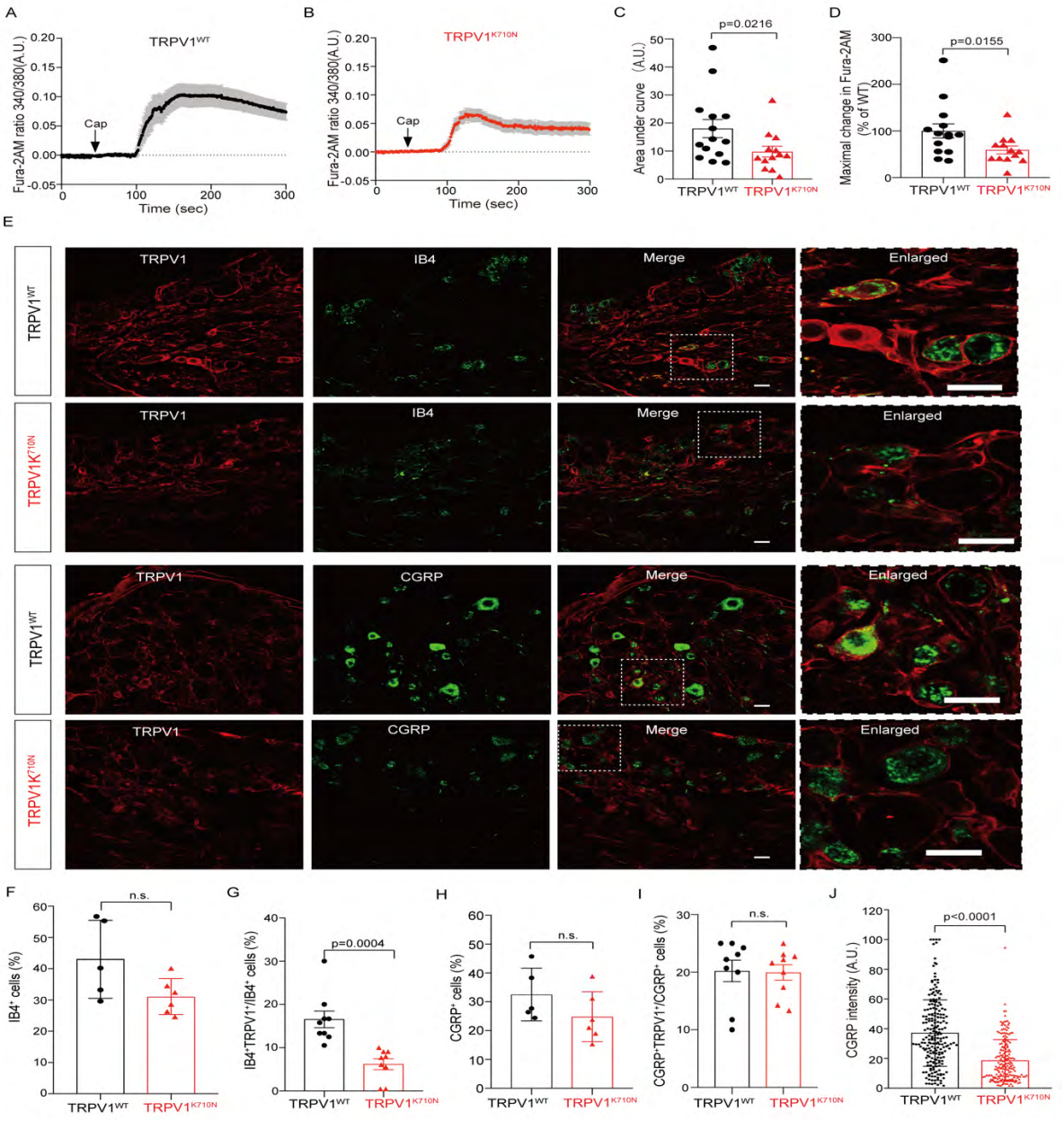

Figure 4 Characterization of TRPV1^{K710N} knock-in mice DRG neurons. (A, B) Changes in Fura-2 AM ratio in response to capsaicin (Cap) in DRG neurons from wild type TRPV1 and TRPV1^{K710N} mice. (C) The area under curve (AUC, total amount of calcium influx) and (D) the % maximal change in calcium influx for TRPV1^{K710N} (n=13) relative to wild type TRPV1 (n=14) from 3 independent experiments. (E) Representative images showing colocalization of TRPV1 with IB4 and CGRP. Bar = 20μm. The total percentage of (F) IB4-positive cells and (G) CGRP-positive cells. (H) The percentage of IB4-positive neurons expressing TRPV1 and (I) CGRP-positive neurons expressing TRPV1. n=5-9 from 3 independent experiments. (J) Fluorescent intensity of CGRP in TRPV1^{K710N} mice (n=202) versus from wild type TRPV1 (n=208) from 3 mice in each group. Data are expressed as mean ± SEM and analyzed using a one-tailed *t* test (C, D) or two-tailed *t* test (F-J).

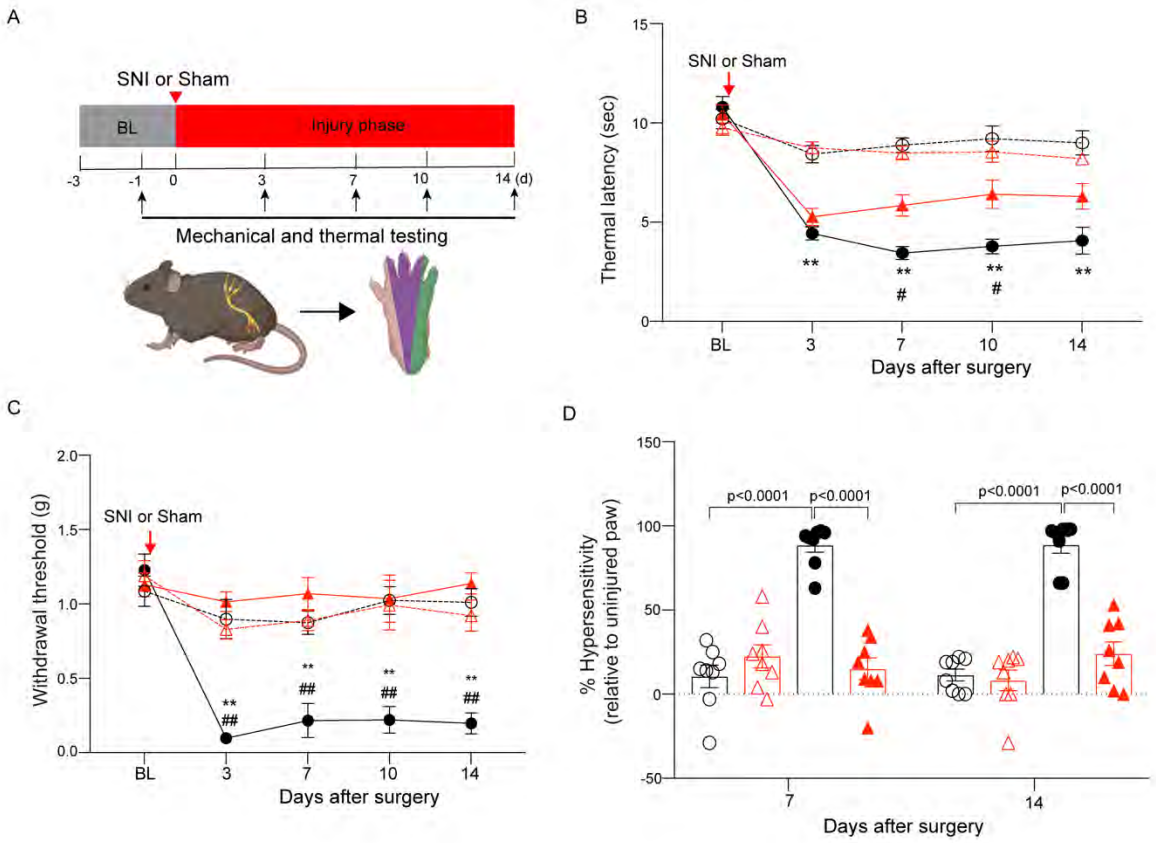

Figure 5 TRPV1^{K710N} knock-in mice are resistant to nerve injury behavior. (A) Experimental protocol for spared nerve injury (SNI) model. Purple: tibial innervated area, green: sural territory (test area). (B) Thermal latency for sham and SNI group. (C) Withdrawal threshold from mechanical stimuli for sham and SNI group. (D) Percent hypersensitivity for sham and SNI group. Data are expressed as mean±SEM, n=8/group. Two-way RM ANOVA analysis followed by Bonferroni's *post hoc* test. **p<0.01, wild type TRPV1 SNI vs. wild type TRPV1 Sham; #p<0.05, ## p<0.01, wild type TRPV1 SNI *vs.* TRPV1^{K710N} SNI. Black dot: wild type TRPV1 mice; Red triangle: homozygous TRPV1^{K710N} mice. Hollow: Sham, solid: SNI.

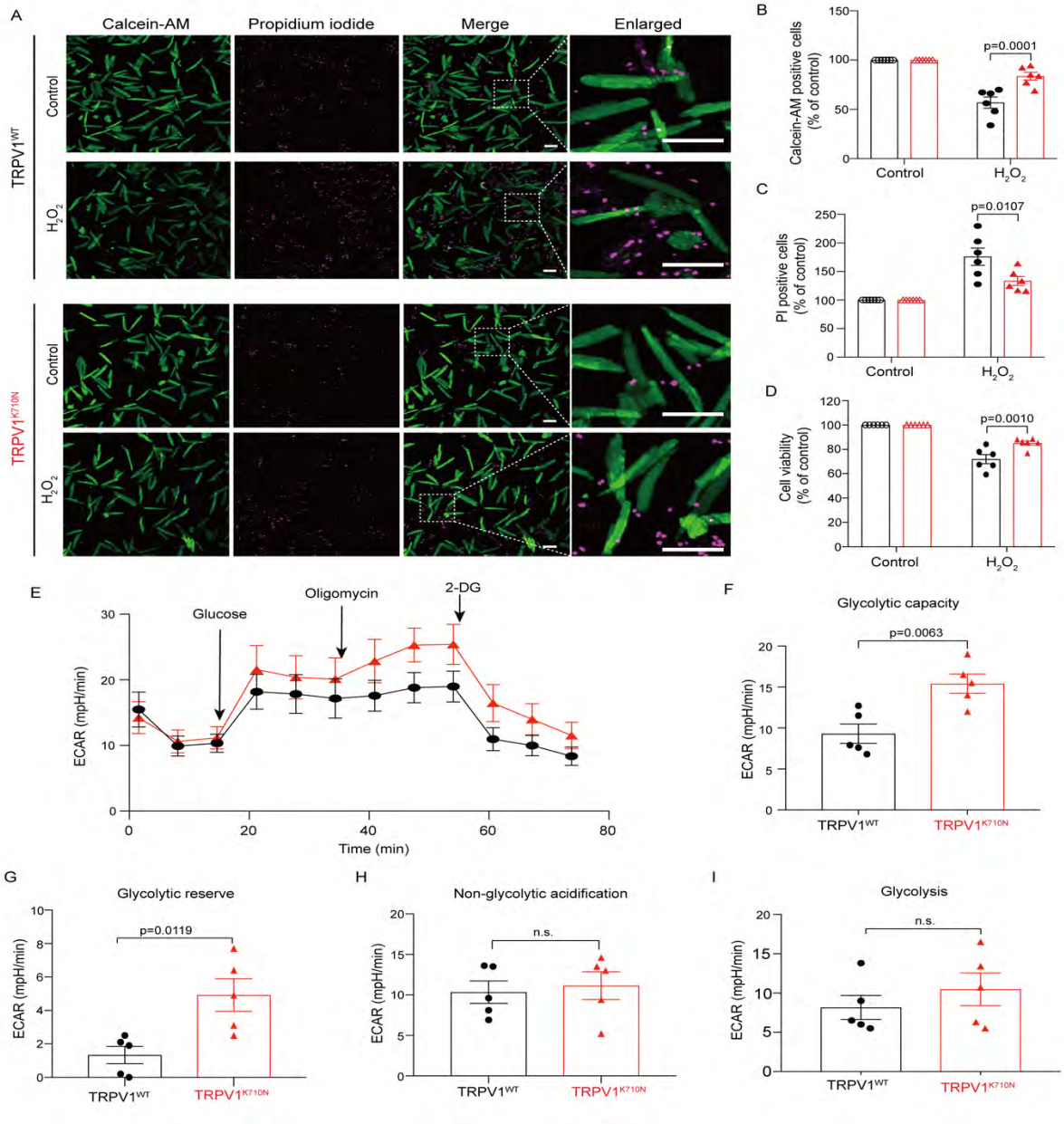

Figure 6 TRPV1^{K710N} knock-in mice cause less cellular injury and improved glycolytic function. (A) Representative images of calcein AM (green) and propidium iodide (PI, magenta) stained cardiomyocytes with or without hydrogen peroxide (H_2O_2) treatment. Bar=100μm. (B) Calcein-AM-stained viable cells or (C) PI-stained dead cells were quantified as the average fluorescence intensity. (D) Cell viability by MTT. The value of control cells in wild type TRPV1 or TRPV1^{K710N} cells was set as 100%, respectively. n=6/group. (E-I) Glycolysis stress test in wild type TRPV1 and TRPV1^{K710N} cardiomyocytes: (E) extracellular acidification rate (ECAR), (F) glycolytic capacity, (G) glycolytic reserve, (H) non-glycolytic acidification and (I) glycolysis. n=5/group. Data are expressed as mean ± SEM. In (B-D), two-way ANOVA followed by Tukey's *post hoc* test. In (F-I), unpaired two-tailed *t* test. Black dot: wild type TRPV1 mice; red triangle: homozygous TRPV1^{K710N} mice.

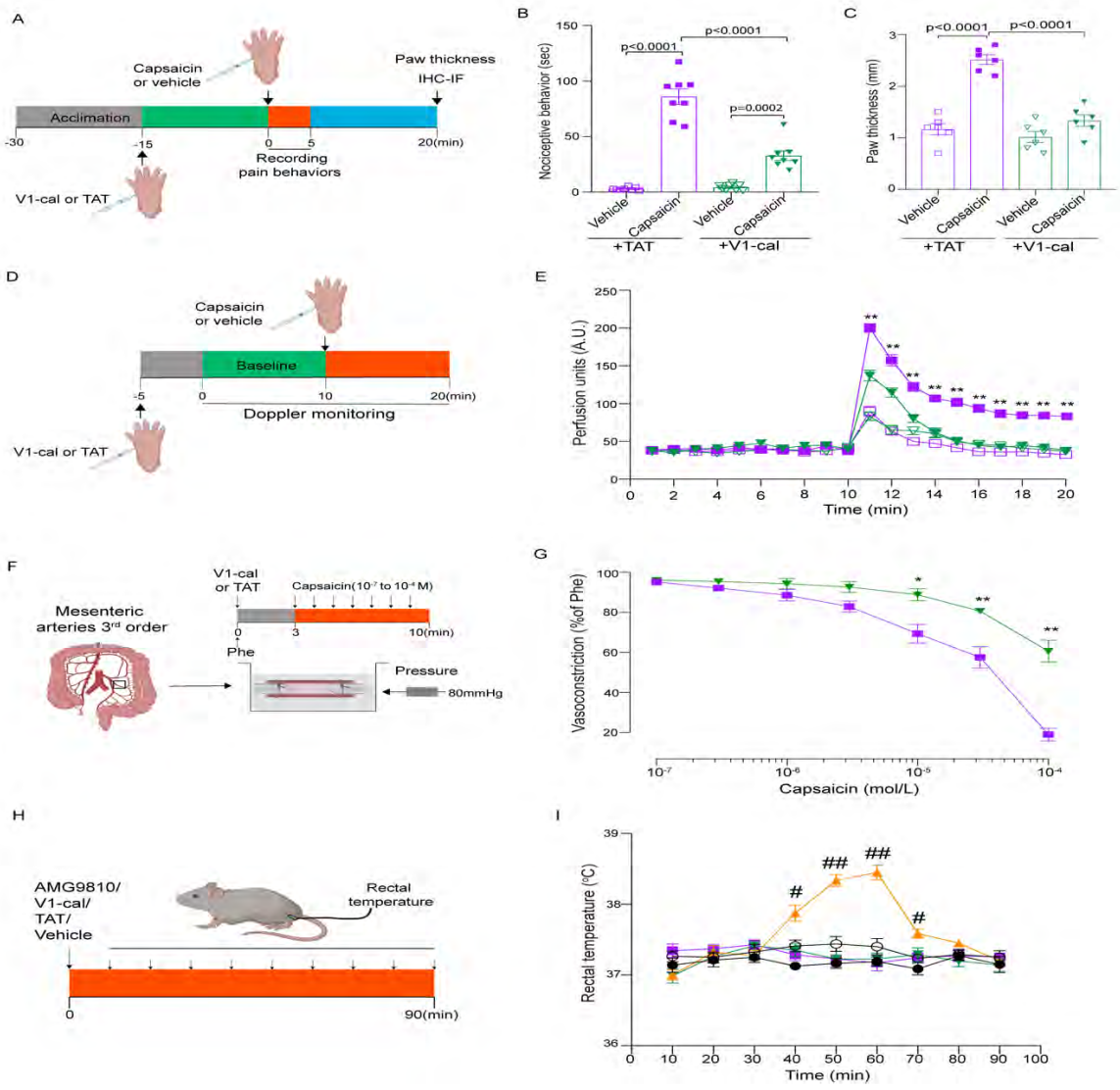

Figure 7 A peptide targeting K710 acutely prevents capsaicin-induced nocifensive behavior and vasodilation without thermal changes. (A) Experimental protocol for peptide treatment before intraplantar capsaicin injection in wild type TRPV1 mice. (B) Nociceptive behavior and (C) paw thickness induced by paw injection of capsaicin after V1-cal or TAT_{47-57} treatment. n=8/group. (D, E) Paw blood flow induced by injection of capsaicin (solid) or vehicle (hollow) in the presence of V1-cal (green) or TAT_{47-57} (purple). (F, G) Pressure myography of mesenteric resistance arteries in response to capsaicin in the presence of V1-cal (green) or TAT_{47-57} (purple). n=6-8/group. (H, I) Body temperature detected by a rectal temperature probe in wild type TRPV1 mice followed by intraperitoneal injection of V1-cal (green), TAT_{47-57} (purple), AMG9810 (yellow), peptide vehicle (saline, solid black dot) or AMG9810 vehicle (5% ethanol in saline, hollow black circle), n=7-8/group. Data are expressed as mean ± SEM. In (B, C), two-way ANOVA followed by Tukey's *post hoc* test. In (E, G, I), two-way RM ANOVA analysis followed by Bonferroni's *post hoc* test. *p<0.05, **p<0.01, V1-cal+capsaicin group *vs.* TAT_{47-57} +capsaicin group; # p<0.05, ## p<0.01, AMG9810 group *vs.* vehicle group.

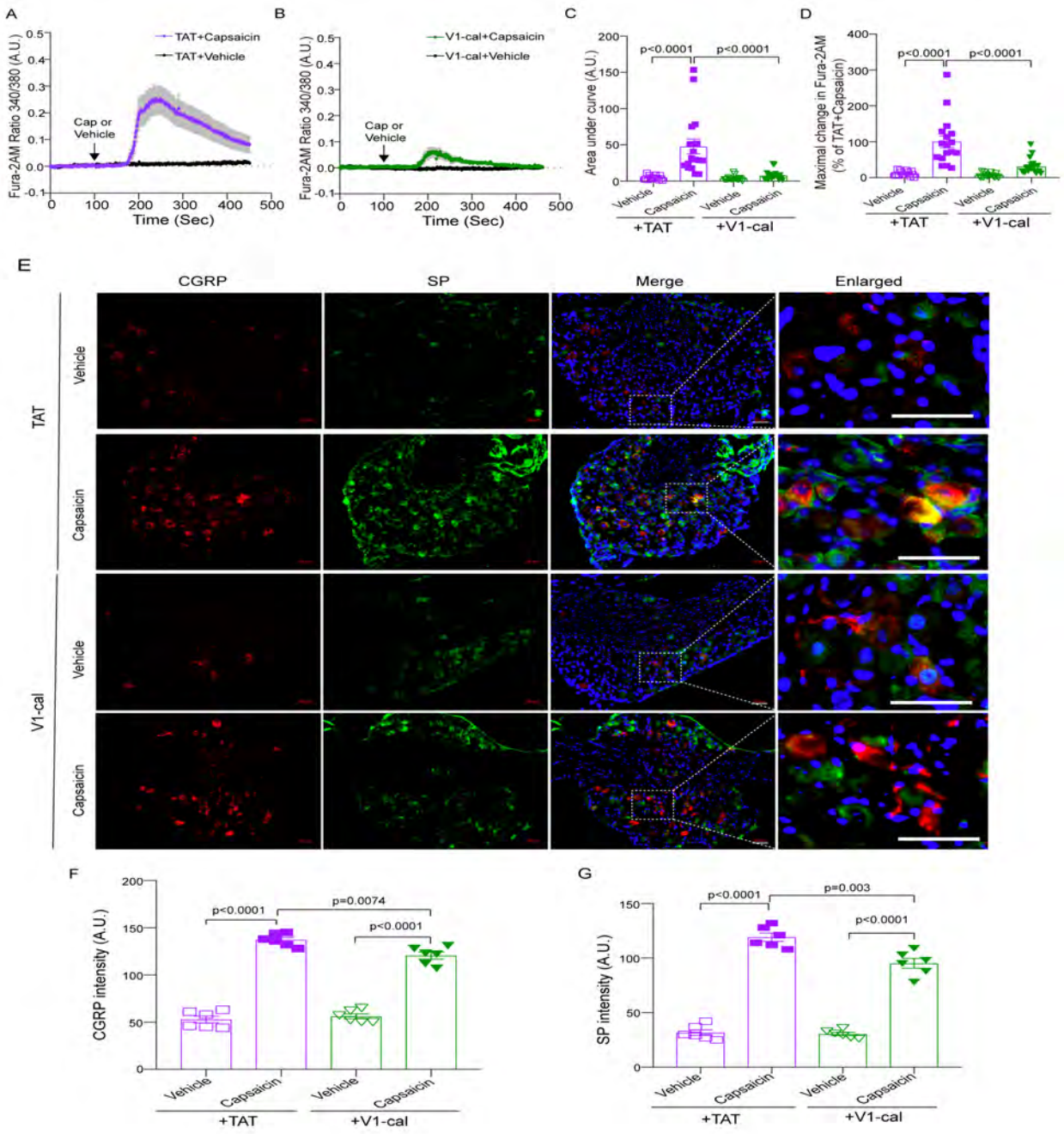

Figure 8. **Impact of V1-cal or TAT$_{47-57}$ on DRG neurons** (A, B) Wild type DRG neurons treated with TAT$_{47-57}$ or V1-cal with and without capsaicin. (C) The area under curve (AUC, total amount of calcium influx) and (D) the % maximal change in Fura-2 to capsaicin-stimulated calcium influx relative to TAT$_{47-57}$. n=16-18 DRG cells from 3 independent experiments. (E) Immunostaining of SP and CGRP in DRG tissues following capsaicin or vehicle injection in the presence of V1-Cal or TAT$_{47-57}$. Bar = 50µm. Quantitative analysis of (F) CGRP intensity and (G) SP intensity in each group. (F, G), two-way ANOVA followed by Tukey's *post hoc* test n=6/group.

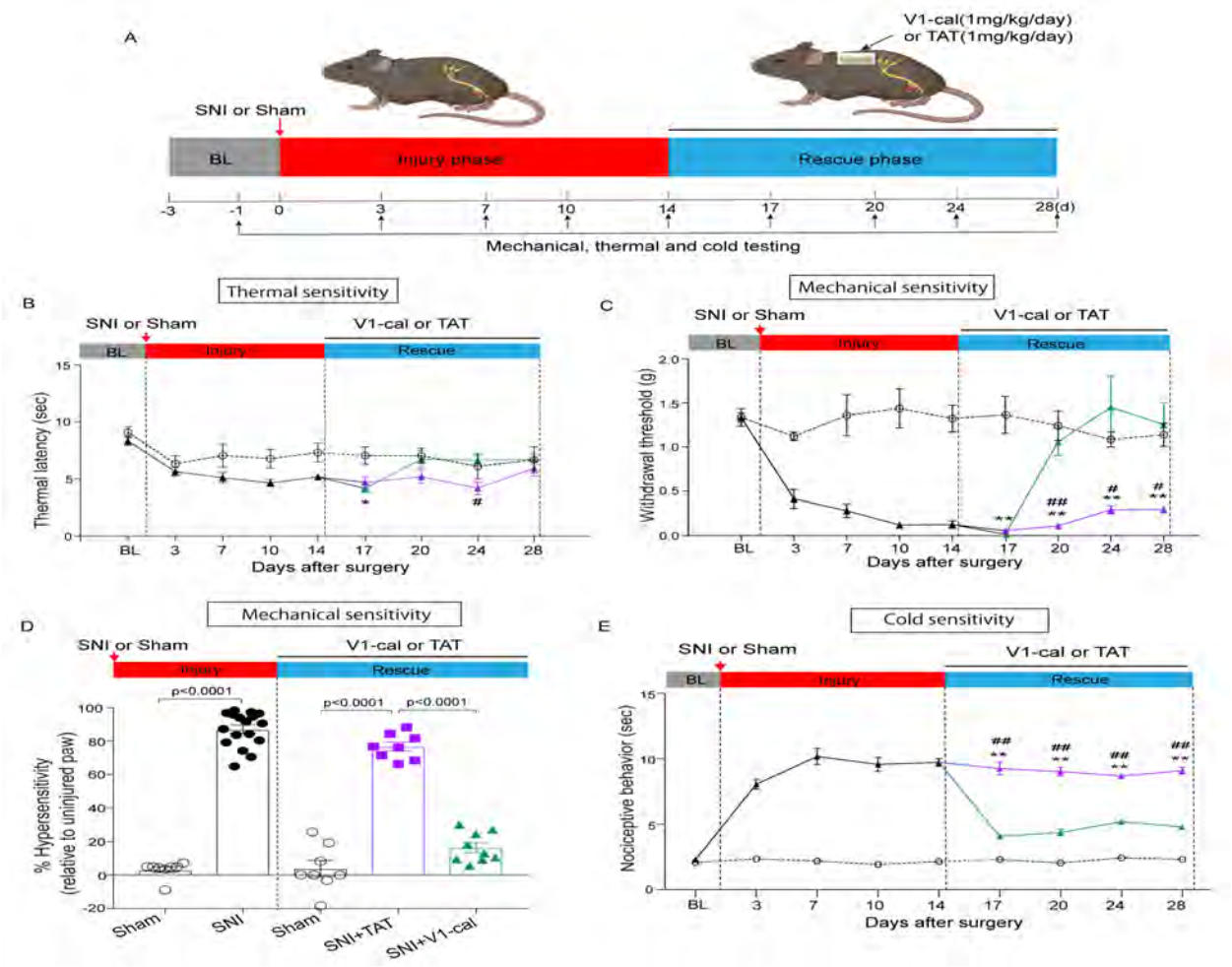

Figure 9 V1-cal rescues nocifensive behavior in wild type TRPV1 mice after spared nerve injury. (A) Experimental protocol for spared nerve injury model with peptide treatment. Rodents underwent SNI and were assessed for 2 weeks (injury phase). After, osmotic pumps were implanted to deliver V1-cal or TAT_{47-57} for two weeks (rescue phase). (B) Thermal latency for sham (dash line) and SNI (solid line) mice. SNI mice were treated with V1-cal (green) or TAT_{47-57} (purple) during rescue phase. (C) Withdrawal threshold from mechanical stimuli for sham (dash line) and for SNI (solid line) mice. SNI mice were treated with V1-cal (green) or TAT_{47-57} (purple) during the rescue phase. (D) Percent hypersensitivity for sham (n=8) and SNI (n=17) mice treated with V1-cal (n=9) or TAT_{47-57} (n=8) during the injury and rescue phases. Data are expressed as mean ± SEM. (E) Nociceptive behavior (paw licking/ flinching) duration from acetone for sham (dash line, n=8) and for SNI (solid line, n=16) mice. SNI mice were treated with V1-cal (green, n=8) or TAT_{47-57} (purple, n=8) during the rescue phase. In (B, C, E), Two-way RM ANOVA analysis with mixed effects model was performed followed by Bonferroni's *post hoc* test. **p<0.01, *p<0.05, SNI+TAT_{47-57} vs. Sham; $^{\#\#}$p<0.01, #p<0.05, SNI+ +TAT_{47-57} vs. SNI + V1-Cal. In (D), unpaired two-tailed t test for injury phase and one-way ANOVA followed by Tukey's post hoc test for the rescue phase.